THE CREATION OF ALL-OXIDE TWO-DIMENSIONAL ELECTRON GASES FOR NEXT GENERATION DEVICES

by

Jason Lynn Stoker

A thesis submitted to the faculty of the
University of Utah
in partial fulfillment of the requirements for the degree of

Master of Science

Department of Materials Science and Engineering

The University of Utah

December 2011

The University of Utah Graduate School

STATEMENT OF THESIS APPROVAL

The thesis of **Jason Lynn Stoker**

has been approved by the following supervisory committee members:

Ashutosh Tiwari	, Chair	**10/28/11** Date Approved
Richard Cohen	, Member	**10/28/11** Date Approved
Michael Scarpulla	, Member	**10/28/11** Date Approved

and by **Anil Virkar**, Chair of the Department of **Materials Science and Engineering**

and by Charles A. Wight, Dean of The Graduate School.

ABSTRACT

Oxide based materials have recently shifted from their traditional passive role as simple insulators, to technologically important active roles. They possess capabilities that semiconductors cannot approach, mainly the ability to couple properties and serve multiple purposes. Oxide based materials, namely the perovskite structure, have strong coupling between mechanical, electrical, optical, and magnetic properties. In most cases these functions can be switched or reversed easily to give the desired property. Piezoelectricity, thermoelectric power, and nonlinear optical affects are a few of the well known oxide roles. However there have been great strides made in oxide electronics, such as high temperature superconductors, colossal magnetoresistance, nonvolatile ferroelectric memory, and the recent advent of 2-dimensional electron gases (2DEG).

The work presented herein focuses on the creation and in depth study of all-oxide 2DEGS. The possible mechanisms that enable two band insulators to conduct metallically at the interface are included in this study.

The bulk of this thesis focuses on two innovative and never before studied uses with oxide 2DEGs. The first novel study is that of thermoelectric power utilizing LAO/STO 2DEGs. These experiments yielded exciting results with very high Seebeck values, the highest being 780 μV/K. This is the first report to indicate the great potential of these devices for thermoelectric power.

The last section focused on theoretical work predicting that an oxide based 2DEG could be made switchable with the application of external electric field. The advent of an all oxide field effect transistor using a quantum confined 2DEG had never been accomplished above the milli-Kelvin range. With the KN/STO material system successful devices were made with the resistance of the film being greatly dependant on the applied field. Furthermore a very unusual low temperature metal-insulator-transition was observed. This report is the first to show these types of results with this material system, or with any all-oxide 2DEG at room temperature.

TABLE OF CONTENTS

LIST OF FIGURES

Figure Page

LIST OF ABBREVIATIONS

AFM	Atomic force microscopy
B	Magnetic Field
CES	Strongly correlated electron system
EDS	Energy dispersive x-ray spectroscopy
e-e	Electron-electron
FET	Field effect transistor
KN	Potassium niobate
LAO	Lanthium aluminum oxide
PLD	Pulsed laser deposition
S	Seebeck coefficient
SEM	Scanning electron microscope
STO	Strontium titanate
TEP	Thermoelectric power
T_C	Curie temperature
UC	Unit Cell
XPS	X-ray photoelectron spectroscopy
XRD	X-ray diffraction

ACKNOWLEDGEMENTS

I would like to personally thank my advisor, Professor Ashutosh Tiwari, for all of his guidance, support and the special opportunities he has provided me. I would also like to thank my committee members, Dr. Scarpulla and Dr. Cohen for their patience, input, assistance and willingness to help. I would also like to thank the aforementioned Professors for all that they have taught me throughout their individual courses, and one-on-one discussion.

I sincerely thank Nathan Gray for his constant assistance and friendship. I would also like to thank the rest of the NMRL members, including Makarand Karmarkar, Micheal Snure, Alan Boardman, and Megan Campbell for all of their help and great company throughout the years. I am especially grateful to Cameron Lewis for his talents and skill sets that he so willingly shared with me. I would also like to thank Nathan Stoker for his help that he so often provided.

I am grateful for both the College of Engineering, and the MSE Department for this opportunity and the assistance. I have enjoyed my relationships with the members of my department and the dean's staff. I personally thank Marilyn Bishop for her help and for always having such faith in me.

For my father and mentor, I thank you so much for your great example, and the countless hours of help and guidance. I am so grateful for all of my parents, Jeanie, Ron, Melanie, Chris, and Debbie, for your never ending support, love, and patience. To my children Alahna and William, thank you for giving me the much needed motivation, joy and love.

Most importantly, I would like to thank my beautiful wife Shelly for everything she has done for me. This educational journey has been tough, and I never would have made it without her, thank you my love, you have always been my inspiration.

CHAPTER 1

INTRODUCTION

1.1 All-Oxide Based Systems

Currently one of the most attractive research topics for Materials Scientists is that of all-oxide based systems. This is mainly due to the exotic and multifunctional properties that they exhibit. In the semiconductor world oxides have always played a passive role, namely as insulating layers. A dramatic role shift has begun for the oxide based systems; they are rapidly changing from passive material layers to functional devices.

1.2 Semiconductors

Semiconductors typically serve a single function, without coupling capabilities. However oxide based systems, especially the perovskite structure exhibit strong coupling nature, including mechanical, electrical, and magnetic properties. The best known example is likely the piezoelectric effect, where mechanical strain induces voltage and vice versa. The piezoelectric effect has been well exploited for use as sensors, actuators, ultrasonic applications, sonar, and transducers. A more recent example is that of perovskite manganites, in which the coupling between magnetic ordering and transport

properties gives rise to the effect of colossal magnetoresistance. The possibility of spintronics is made possible only through the use of oxides, due to the degree of spin polarization and the susceptibility of these oxides to a magnetic field. Oxides are also the leading materials type for high temperature superconductivity. Another one of the most intriguing oxide couplings is that of nonlinear optical behaviors, such as second harmonic and sum frequency generations that have enabled great advances in laser and LED wavelength capabilities. One material seems to stand out from the other oxides; strontium titanate (STO) has become analogous to Si use in semiconductors, as it is probably the most widely used substrate material for oxide research and device development. There are many more material systems and an unknown number of uses for actively functioning oxides. More are being developed daily, yet the scope of this thesis is not to cover all oxide-based systems or applications.

1.3 The All-Oxide Based 2-Dimensional Electron Gas (2DEG)

Recently a metallic conduction channel was discovered at the interface of two large gap band insulators. This channel is referred to as a 2-dimensional electron gas (2DEG). Physics explains the phenomenon as a quantum well in two dimensions (x-y) but lacking the third z dimension. This was first discovered by using ultrathin films of lanthanum aluminum oxide deposited on STO.[1] High mobility, high carrier concentrations, and extreme resistance values were initially reported, and as more and more groups have joined in the research of this system better and better results are reported. It must be noted however that the true mechanism/s responsible for this

conduction pathway is hotly debated and still remains unknown. Chapters 2 and 3 will cover more of this debate and the leading theories.

The topic of this experimentally based thesis is the study of the LAO/STO 2DEG system, some of the assumed surface properties considered necessary (i.e., sharp, abrupt interface), and an unexplored use for the newly discovered system, thermoelectric power. This thesis also investigates a new and novel 2DEG material system, the use of a ferroelectric potassium niobate (KN) as the thin film on STO. Following some theoretical work that proposes the device could produce a 2DEG that has the ability to switch conduction states, in essence an all-oxide field effect transistor (FET).[2]

In Chapter 2 the background on the materials and the theories are presented, along with a detailed description of the experimental setups/procedures used.

An investigation into the LAO/STO 2DEG system is investigated in Chapter 2. The substrate surface requirements are put to the test, in order to see if quantum confinement is truly occurring or if other conduction mechanisms are at work. A thorough electrical characterization of the films reveals the carrier concentrations, mobilities, activation energy of thermal carriers, and the resistance values. All of the electrical tests were performed in wide temperature range of 300-10 K.

The novel use of LAO/STO 2DEGs as a potential thermoelectric material was researched in Chapter 4. Several of the samples created for the study in Chapter 3 were again utilized for the measurements of the Seebeck coefficient, which is a measure of the voltage developed across the sample from a given temperature difference.

Chapter 5 researches the aforementioned theory of ferroelectric films to produce switchable 2DEG devices. This study focused solely on the ferroelectric material

potassium niobate. Resistance vs. temperature measurements were performed to prove/disprove the theorized possibility of low temperature superconductivity. A thorough investigation into the resistances dependence on an applied external electric field was also performed.

1.4 References

1. Ohtomo, A.; Hwang, H. Y., A high-mobility electron gas at the LaAlO3/SrTiO3 heterointerface. *Nature* **2004,** *427* (6973), 423-426.

2. Wang, Y.; Niranjan, M. K.; Jaswal, S. S.; Tsymbal, E. Y., First-principles studies of a two-dimensional electron gas at the interface in ferroelectric oxide heterostructures. *Physical Review B - Condensed Matter and Materials Physics* **2009,** *80* (16).

CHAPTER 2

BACKGROUND AND EXPERIMENTAL TECHNIQUES

2.1 Theoretical Criteria for Oxide Based 2DEGs

Currently oxide-based 2DEGs have only been produced using pulsed laser deposition (PLD) and molecular beam epitaxy (MBE), with most of the successful 2DEGs being produced by PLD. Both theoretical and experimental work describes the need to have an atomically abrupt and sharp interface between film and substrate. Perovskite structured oxides have been the only materials to illustrate this phenomenon.

Furthermore, the Perovskite substrate must have an all-A or all-B terminated surface. There is a need for a polar discontinuity between film and substrate. The only successful all-oxide 2DEGs have been constructed using a nonpolar substrate and a polar thin-film for example LAO/STO. In addition, a range of oxygen partial pressures down to 10^{-6} torr is required for the least resistive 2DEG to form in the laboratory.[1]

2.2 The Perovskite Structure

Perovskites were first discovered in the Ural Mountains of Russia by Gustav Rose in 1839 and were named after Russian mineralogist L. A. Perovski. Unlike traditional semiconductors which have a single functionality, the perovskite crystal family possesses multi functionality including the coupling between mechanical, electrical and magnetic properties. This gives rise to many unique and exciting properties including ferroelectricity, piezoelectricity, nonlinear optical properties, high Tc superconductivity, insulating conduction, metallic conduction, multiple magnetic states, colossal magnetic resistance and high dielectric constant. These properties are greatly influenced by doping the substrate with small amounts of dopants and or lattice strain. Close lattice matching between perovskites gives the ability for epitaxial growth on other perovskite substrates. Most recently this ability for lattice matching has given rise to the topic of this thesis, oxide 2-dimensional electron gases.[1]

The perovskite structure is a special combination of face-centered and body-centered cubic structured units. Two ways of viewing this structure are shown in Figure 2.1. The oxide structure can be written in the form ABO_3, where A ions sit at the corners of the cube, O ions sit on the faces, and B ions reside in the center of the cube, which is an octahedral site. Most perovskite types have a large metal ion as A, and, typically, a small transition metal ion with a high positive oxidation state as B. The relative small size of B and the large octahedral site in which it resides give the B ion a unique ability to move or shift slightly when an electric field is present. The bulk effect of the highly charged ions simultaneously shifting when an electric field is applied results in high polarization; this is referred to as a high dielectric constant.

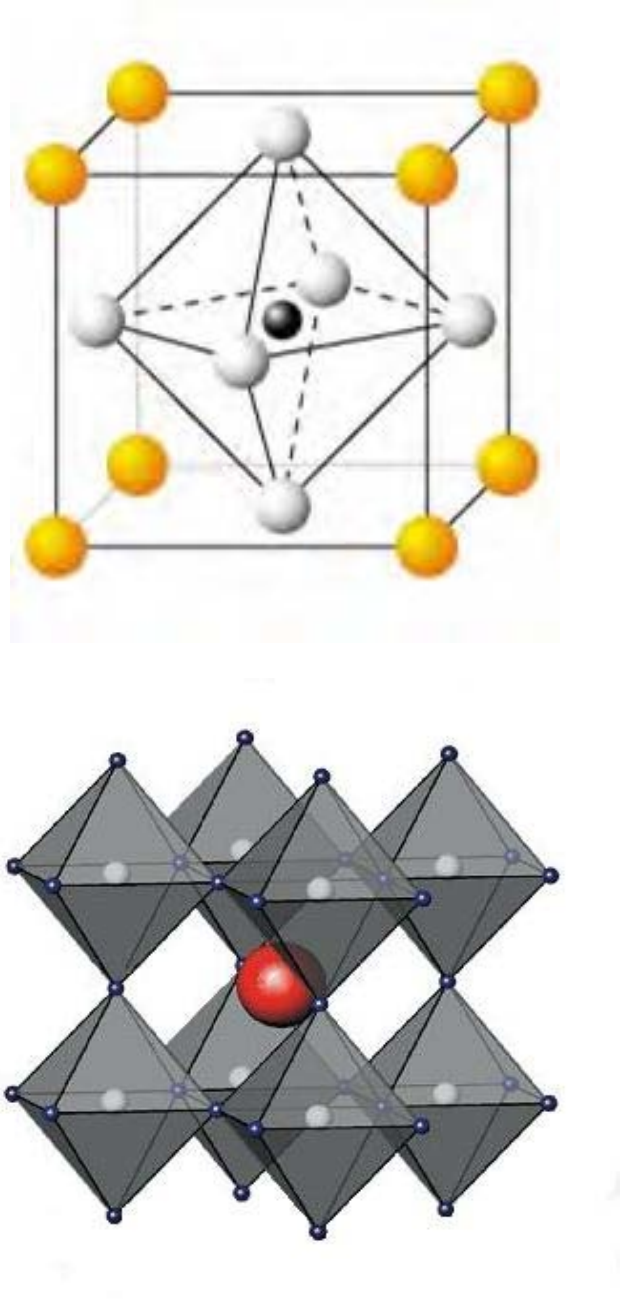

Figure 2.1 Illustrating two separate views of the ABO_3 perovskite structure.
Top: A ions (yellow) sit at the corners of the cube, O ions (white) sit on the faces, and B ions (black) reside in the center octahedral site.
Bottom: A ions (red) sit at the corners of the cube, O ions (blue) sit on the corners, and B ions (white) reside in the center octahedral site.

Possessing a high dielectric constant means that the material can store an electric charge; thus giving rise to capacitance.

Another unique property of the perovskite structure is the ability to easily substitute A and B sites. Furthermore, perovskites maintain their structure despite large amounts of oxygen vacancies in their structure.

2.3 Materials Properties

2.3.1 Strontium Titanate ($SrTiO_3$) Properties

Historically, strontium titanate (STO) was used as a substitute for diamonds in the jewelry industry prior to the discovery of cubic zirconia. Currently, STO is an extremely important substrate and is the workhorse of all oxide-based research.

STO possesses many desirable properties. It has a high melting temperature that is 2080°C. When STO is in stoichiometric proportions it has an insulating material. However, when it possesses high oxygen vacancy or is doped with Nb or La it becomes metallically conductive.[2] It has a refractive index of 2.41 and because of this it was used as a substitute for diamonds in the jewelry industry prior to the discovery of cubic zirconia. STO becomes superconductive when it is below 350mK. It is optically transparent when it is in stoichiometric proportions. STO has high photoconductivity and can behave like a metal. Its dielectric constant at room temperature is 300 and increases to 10,000 at low temperatures.[3] The thermal conductivity of STO is 12 W/m K. STO has a cubic structure with a lattice parameter of 3.905 A. It is nonsecular polar between layers and possesses a wide band gap of 3.2 eV. In oxide research STO is analogous to Si as the workhorse substrate.

2.3.2 Lanthanum Aluminum Oxide ($LaAlO_3$) Properties

Lanthanum aluminum oxide (LAO) is an important substrate for high Tc superconductors, magnetic and ferroelectric thin films. LAO possesses a wide bandgap of 5.5 eV; it has a nontemperature dependent dielectric constant of 24. Thus it is an insulating material which is polar between layers. It has a cubic structure with a lattice parameter of 3.821 Å in a temperature range of 25 to 435 K.

2.3.3 Potassium Niobate ($KNbO_3$) Properties

Potassium niobate (KN) is typically exploited for its nonlinear optical (NLO) properties. These include birefringence, second harmonics and some frequency generation with nearly 100% efficiency.[3] KN has an orthorhombic structure where a and c are 3.969Å and 5.726Å, respectively. KN possesses phase transitions similar to barium titanate (BTO) which are tetragonal to orthorhombic to cubic at -50°C; 220°C; 430°C, respectively. KN has a dielectric constant of 200 to 800.[3] Because of its noncentro-symmetry KN is both ferroelectric and piezoelectric.

The difficulty with both thick and thin film potassium niobate is the volatility of potassium. When thin films containing potassium are produced they typically result in non-stoichiometric films. A thorough study of potassium deficiency was conducted by Yang et al.[4]

The band gap of KN is generally reported as 3.2 eV. However the structure of KN yields an anisotropic band gap (birefringement nature). Through UV-VIS spectroscopy the author has found the band gap to be 3.85 eV and 4.12 eV in the <001> and <111> directions, respectively.

2.4 Materials Preparation

2.4.1 Substrate Preparation

One square centimeter of strontium titanate (STO) substrates (100) were purchased epi-polished from MTI. The substrates were first cleaned ultrasonically in an acetone bath. In order to render the STO substrate all B (Ti) terminated, a process of preferential Sr etching was utilized. This was accomplished by submersion of the substrates in an HF solution. A (Sr) site termination was achieved by preferential etching of Sr followed by deposition of a monolayer of Sr via PLD.

2.4.2 Target Preparation

A single crystal of LAO was purchased from MTI, for target use. As single crystal potassium niobate (KN) is extremely hard to come by, it was necessary to produce dense ceramics targets. Puratronic® grade potassium niobate (99.999%) powder was purchased from Alfa Aesar. X-ray diffraction (XRD) was conducted on the as-received powder for later particle size comparison. The powder was placed into an M18 Sweco Vibratory Mill for attrition milling with solvent and zirconia media 2 mm in diameter for a 24-hour period. The powder was then strained using a sieve with 45 micron openings. The media were rinsed thoroughly and the remaining solution was dried with the assistance of flowing air. The powder was then sieved again through the 45 micron sieve to break up any conglomerates. XRD was also performed on the precalcined powder utilizing a Phillips PW 3040 for later comparison.

The powders were then formed into pellets via pressing uniaxially in a one-inch die at 30 MPa, then cold isostatically pressed (Autoclave Engineers CIP) at 241 MPa for

15 minutes. The resulting discs were calcined at 950° C for 12 hours encased in a native powder bed. To ensure the powders were fully calcined the process was repeated by pulverizing the pellets to a fine powder. An XRD scan was completed at this intermediate step also. New discs were made following the above procedure and calcined at 900° C for 12 more hours. A novel encasement of the pellets was developed to prevent potassium loss during sintering, which consisted of:

- A thick powder bed consisting of the native unmilled powder bed compressed around the pellet.
- A small handmade gold crucible filled with potassium super oxide (KO_2) was placed on top of the powder bed to create a potassium rich atmosphere.
- The ceramic crucible was lidded then extra thick zirconia discs placed on top to add extra downward pressure on the lid seal.
- This crucible was then placed on top of a second crucibles' lid and the second crucible was inverted to seal.
- Dense alumina plates capped the outer crucible to make a tighter seal.

2.5 Experimental Design and Development

2.5.1 Shadow Mask Design

Following the work done by Ohtoma et al., a six probe Hall geometry was chosen for the construction and testing of the LAO/STO 2DEGs.[1] This was accomplished using a two-step contact shadow mask procedure utilizing a theta z mask aligner for the device design. In order to ensure interfacial contact an overlapping contact design was chosen. This design enabled two methods for interfacial contact: First, direct edge contact, and

second, the diffusion of Pt through the ultrathin films. Others have reported the need for laser/thermal annealing of the contacts, and Ar ion etching down to the interface. The authors chose a two-prong method for interfacial contact. The platinum overlaps the film and substrate continuously for direct edge contact (Figure 2.2). Furthermore the author's experience has shown that Pt will make contact with the substrate surface through the film (even if this is not desired) directly with higher fluence PLD. The films were deposited via PLD using a single crystal LAO target, followed by the deposition of Pt contacts without breaking vacuum.

2.5.2 PLD In Situ Mask Aligner

The mask design chosen presented the obstacle of depositing multiple layers in the PLD without repeated heating/cooling and vacuum breaking cycles. To accomplish this the existing rotational shutter feed through had to be replaced with a theta, z feed through. This type of feed through enables both rotational motion and the ability to pull and push the shaft deeper into the vacuum chamber. A four arm (cross) shape was decided upon. Two of the arms were milled to specifically hold the one inch square masks, while one was left solid for use as a shutter, and the last was left open to enable depositions over the entire surface of the substrate. In order to align the masks with great accuracy an alignment pin was placed on to an altered substrate heater surface. The author designed the system and had milled with great accuracy through wire EDM. A detailed pull-apart schematic and an image of the mask aligner can be seen in Figure 2.3 and 2.4, respectively.

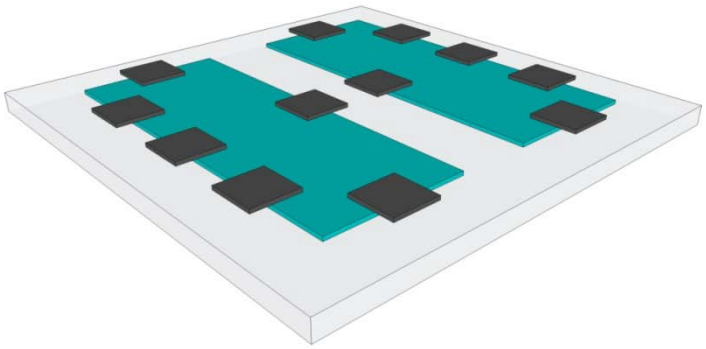

Figure 2.2. Schematic illustration of the thin film device construction. Teal represents LAO and dark grey represents platinum; the base substrate is STO. (Designed by author)

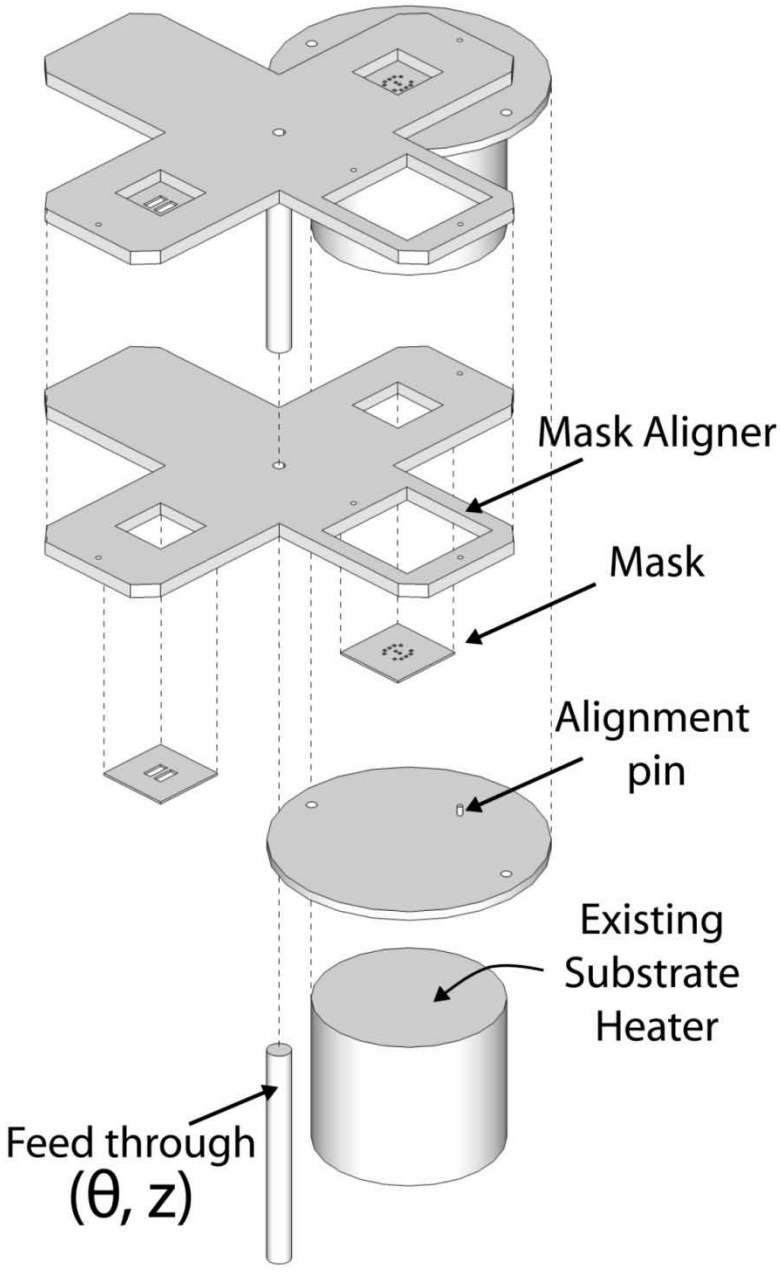

Figure 2.3. Pull apart schematic of the mask aligner and existing substrate heater. (Designed and built by author.)

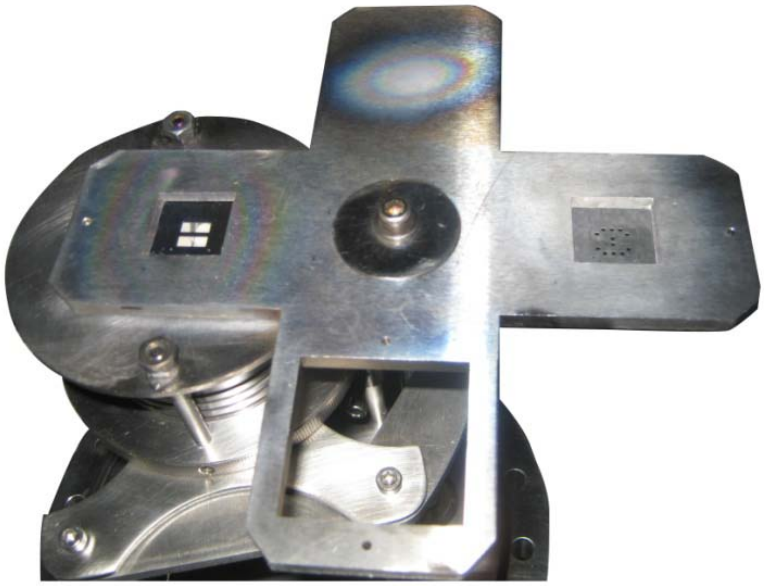

Figure 2.4. Image of the installed and well functioning *in situ* PLD mask aligner. (Designed and built by author.)

2.5.3 PLD Cold Finger Design

An evaporative liquid nitrogen 'cold finger' was designed and built by the author to enable low pressures (10^{-6} torr) during ablation while the substrate heater is on. This was accomplished by creating an airtight feed through and into the PLD vacuum chamber. The feed through was built with two 3/8" diameter stainless steel pipes welded two a 6 bolt flange. A large coil of copper pipe was attached to the interior feed through pipes. The exterior pipes also transitioned to copper and were soldered to a large copper dewar, with one opening being flush with the bottom of the dewar, and the other attached to a threaded fitting to enable a vacuum to be pulled. Although copper is a major heat sink it was chosen for the ease of air tight construction, namely soldering. The dewar was then encased in a cylinder with about a two-inch gap between them. Polyurethane foam was used to insulate the dewar from the surroundings. Pictures of the internal components and the complete installed unit can be seen in Figures 2.5 and 2.6, respectively. Prior to installation of the cold finger only a base pressure of 10^{-6} torr was attainable with the system on hand. However when the substrate heater is at temperature, and ablation is occurring the pressure would rise to $10^{-5} – 10^{-4}$ torr. After installation of the cold finger a pressure of 10^{-6} torr could be maintained throughout the deposition.

2.5.4 Testing fixture design

PCB circuit testing circuits were designed to hold the devices securely and enable the ability for wire bonding, thus eliminating the chance for human error when making indium dot contacts. The testing circuits were produced via photolithography and etching

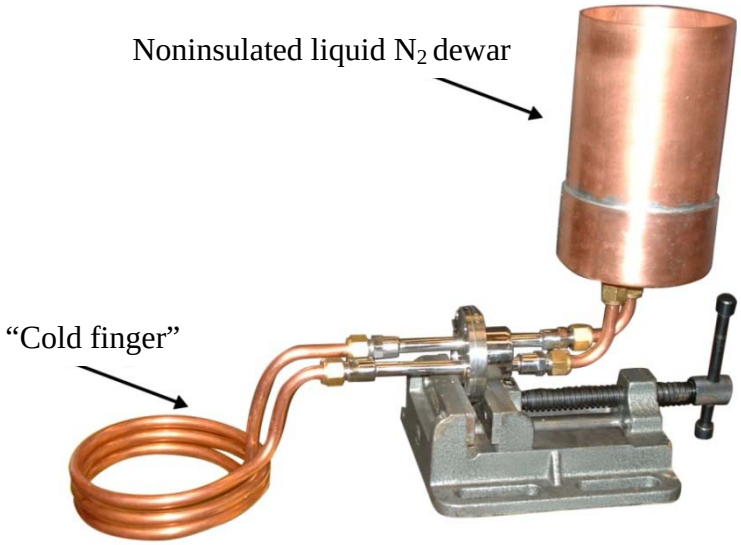

Figure 2.5 Picture of the interior construction of the cold finger design illustrating the surface area of the coils. (Designed and built by author.)

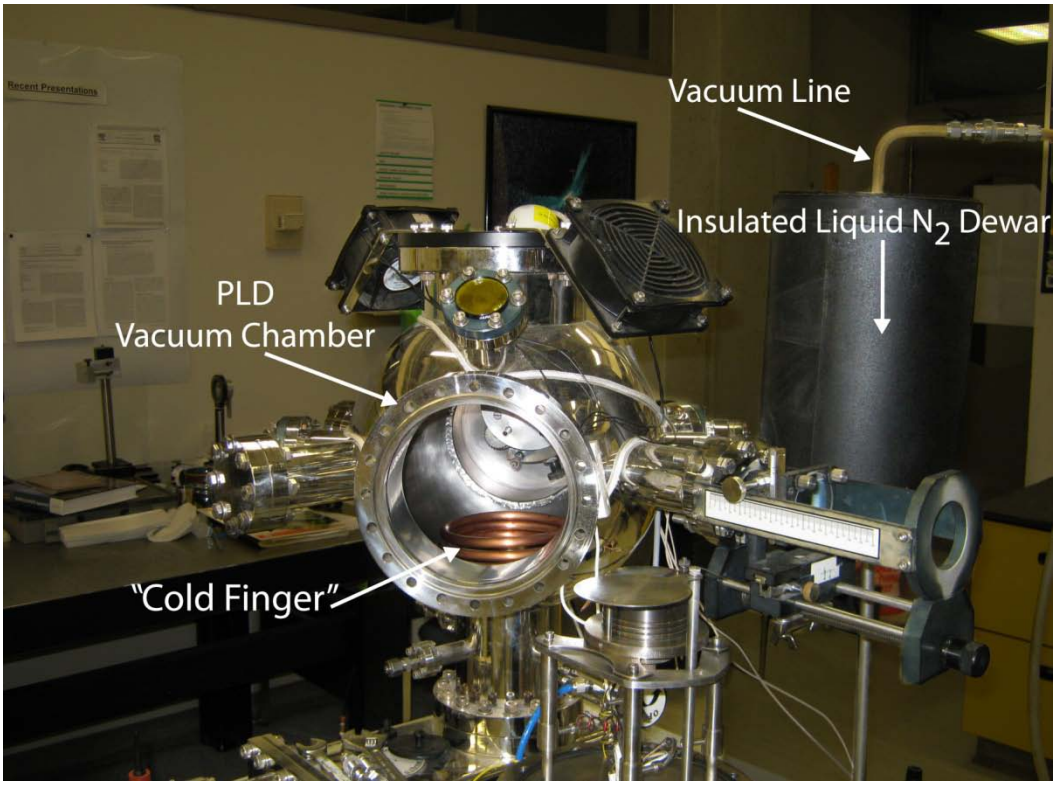

Figure 2.6 Picture of the complete PLD system, this image illustrates the cold finger after installation.

process. The design enabled easy testing of both the devices while keeping the devices and the fragile bond wires. The testing circuits were designed to fit the stage of a liquid helium closed cycle cryostat. A direct thermal contact was created between the top and bottom of the PCB circuit directly below the substrate to ensure temperature accuracy during measurements. This was done with a thick mixture consisting mostly of 100 μm copper powder with flux. This mixture was then tightly packed into a predrilled hole, and solder was then applied to complete the thermal contact. The top and bottom copper surfaces of the PCB were 200 μm thick, which possesses a thermal conductivity of 400 W m^{-1} K^{-1}. The thermal bridge between the surfaces was mostly copper with binding solder; the thermal conductivity of the thermal bridge follows the rule of mixtures as seen in Equation 2.1.

$$k_T = xk_{Cu} + (1 - x)k_s \tag{2.1}$$

where k_T , k_{Cu} , k_s represent the thermal conductivities of the total, copper and solder, respectively. The x symbol represents the volume fraction. Weights of the board with copper packed in before and after solder knowing the density of solder, the volume fraction of copper was found to be around 0.93. Knowing the thermal conductivity of solder to be 50 W m^{-1} K^{-1} the above equation yields a total thermal conductivity of the thermal bridge to be 330 W m^{-1} K^{-1}. With these high values of thermal conductivity between the device and the cryostat stage it is easily assumed that thermal equilibrium exists. A schematic and picture of the 2DEG testing fixtures are shown in Figures 2.7, 2.8.

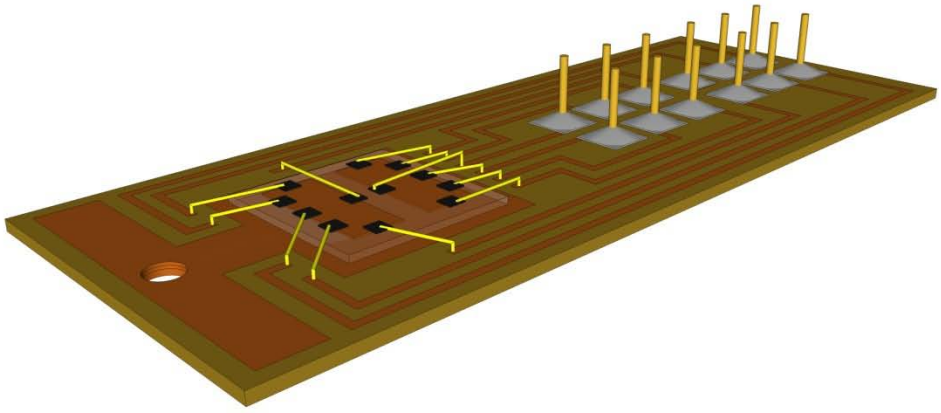

Figure 2.7. Schematic illustration of the testing fixture designed for electrical characterization of the 2DEGs.

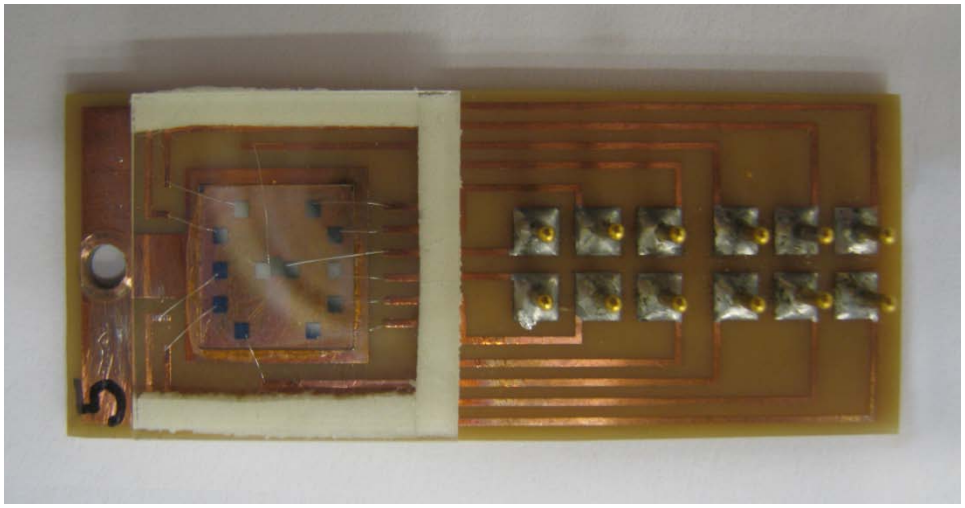

Figure 2.8. Picture of a complete device mounted and wire bonded to the testing fixture, with a protective glass cover installed. (Designed and built by author.)

2.5.5 Thermoelectric Testing Fixtures

The thermoelectric testing fixtures followed the same photolithography/etching process as previously discussed. The difference in testing fixtures was the need to limit thermal contact to the cryostat to one side of the substrate. In order to accomplish this several alterations to the previously made testing fixtures had to be made. In order to limit the thermal conductance through the PCB board the copper on top and bottom of the circuit were limited to one side of the device, with the same type of thermal bridge on the one side. Furthermore a gap was milled to create a separation between the hot and cold sides. The underside of the circuit was milled to one half of the thickness on the 'hot' side of the device. This was done in order to ensure no contact between the circuit and the cryostat stage in that area. Furthermore, directly underneath the hot side of the substrate the circuit board was milled even thinner, to 1/3 of the original thickness. On the hot side of the circuit board resistive heaters were placed directly under the substrate. In order to ensure accurate temperature measurements at both ends, two Si diodes were placed directly on top of the substrate. A schematic of the resulting testing circuit is shown is Figure 2.9.

2.6 Creation and Physical Characterization of Oxide 2DEGs

2.6.1 Pulsed Laser Deposition

All of the thin films produced herein were done utilizing the nonequilibrium method of pulsed laser deposition (PLD).[5] In the PLD technique a 25 ns pulsed excimer laser (λ=248 nm) is focused at a 45° angle onto a solid target. The energy densities ranging from 1-6 Jcm^{-2} can deliver up to a GW/ cm^{-2} to the target, which creates a

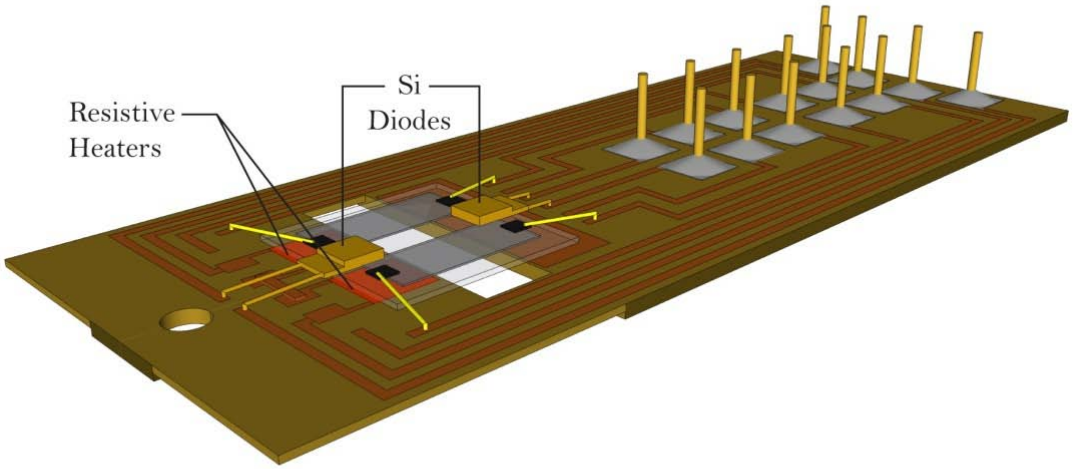

Figure 2.9. A schematic illustration of the thermoelectric testing fixture. The schematic indicates the placements of the onboard resistive heaters and the diode positions. (Designed and built by author.)

localized temperature around 25000 K.[5] This intense heat ablates the surface atoms instantly and retains the stoichiometry of the target regardless of the melting point of the constituent atoms.[5] The supersonic jet produced expands normal to the surface of the target and behaves like a gas expanding in vacuum. This plasma contacts the heated substrate with sufficient energy to order itself and produce textured or epitaxial films as it condenses back to a solid at the relatively cold surface. Another advantage of the PLD technique compared to other thin film processes is the relatively low substrate temperature needed to achieve epitaxy.

The PLD system used for this study was a Compex Pro 205 KrF excimer laser with 248 nm wavelength and 25 ns pulse width. The PLD chamber has the ability to deposit at a variety of pressures and substrate temperatures ranging from 10^{-6} – 10^{-2} torr, and room temperature to 850° C, respectively. The PLD chamber has the ability to hold six targets at once and the ability to auto switch between them; the targets are rotated at 3 RPM in order to prevent localized heating of the target. A schematic of the PLD system is shown in Figure 2.10.

2.6.2 X-ray Diffraction

X-ray diffraction (XRD) with Cu Kα source and Ni filter was used to perform θ-2θ° scans of the powders, targets and thin films. XRD is used to determine crystal phases present, their orientation, the lattice parameters, and the full width half max (FWHM). FWHM can be used with the Scherrerr formula to determine grain/particle size, as the broadening of the peaks indicates a reduction in size. The XRD that was used to perform

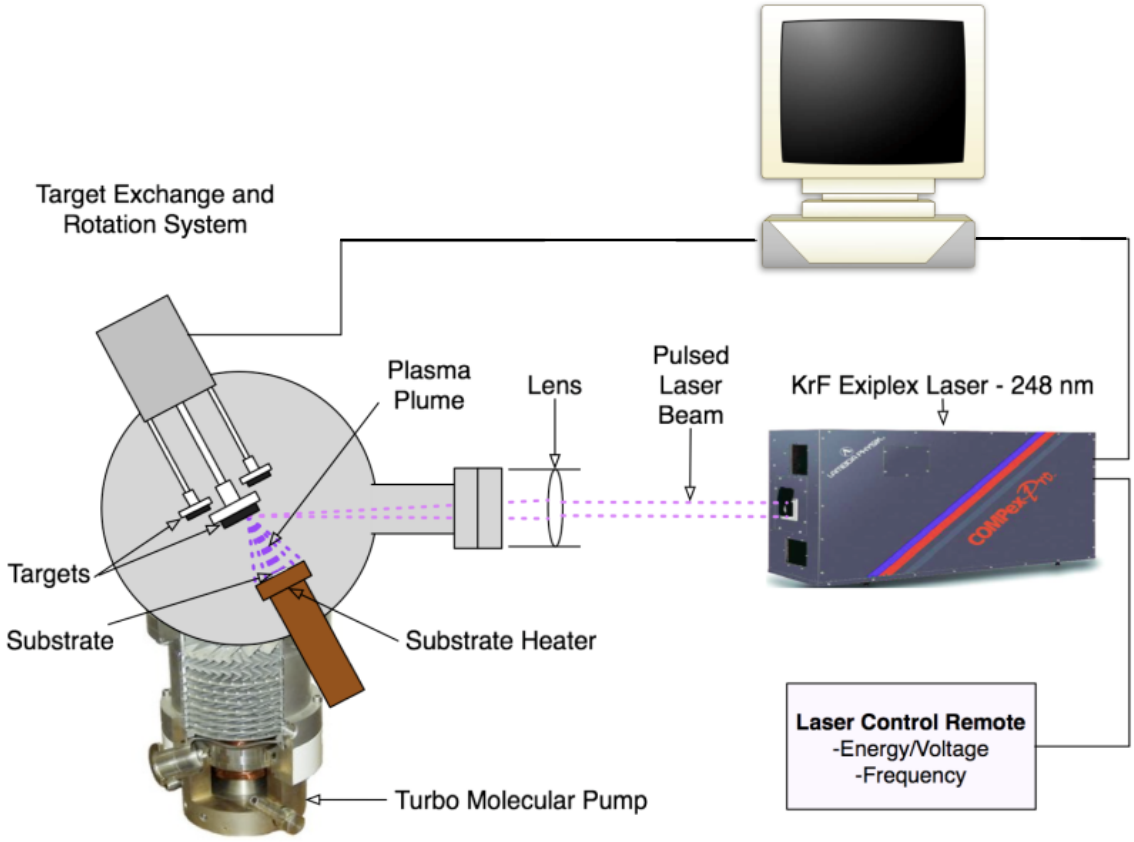

Figure 2.10. A schematic illustration of the pulsed laser deposition system used for the thin film research contained herein.

this procedure was a Philips X'pert diffractometer generating x-rays from a Cu Kα source with a wavelength of 1.5406Å. Unfortunately this XRD used does not possess the ability to perform phi theta scans, this greatly hindering the ability to distinguish between a highly textured, and an epitaxial film.

2.6.3 Atomic Force Microscopy

Atomic force microscopy (AFM) was used to characterize the surface of the substrates, thin films, and film thicknesses. A Bruker Dimension ICON-PT AFM in tapping mode measured the RMS surface roughness of the substrates and thin films. The AFM technique uses a Si probe with a 5 nm tip. A laser is reflected off of the probe tip as the cantilevered Si tip is deflected by the surface roughness. This deflection is observed by the laser. The AFM used for this characterization possesses subatomic resolution for detecting surface features.

2.6.4 Profilometry

Profilometry was used in conjunction with AFM to verify the height of the thin films. The profilometer used was a Tencor P-10. The profilometer uses a mechanical method to find the line profile of a sample using a stylus tip.

2.7 Electrical Characterization of Oxide 2DEGs

2.7.1 Resistance vs. Temperature

Measurements of the resistance vs. temperature reveals whether the material's conduction behaves as an insulator, semiconductor, or a metal. This information is easily

extracted from the shape of the plot that is produced, as each type has a distinct shape (see Figure 2.11). The measurements were taken by mounting the testing circuits onto the stage of a Janis 22 closed cycle liquid helium cryostat. A roughing pump provides the initial vacuum. Once a temperature of 200 K is reached the vacuum valve is closed and charcoal getters decrease the vacuum even further. The temperature range of the cryostat used is 340 K – 10 K. The resistance versus temperature measurement was made fully automatic using Labview to control all of the components. A Lakeshore 352 temperature controller is at the heart of the system. Four probe resistance measurements are taken which eliminates the additional resistance from the ohmic contacts (see Figure 2.12). A Keithley current source drives a constant current, while a Keithley nanovoltmeter records the data. The Labview program converts the voltage and current into a resistance value, which is plotted against the temperature.

2.7.2 Hall Measurements

Hall measurements provide valuable information about the type of carriers (holes or electrons) present in the material being tested. The driving force for the Hall measurement is the interaction between a moving charged particle and an applied magnetic (B) field. As the electrons/holes travel through the sample while a B-field is applied perpendicular to the line of travel and normal the surface of the material, a torque is applied to the moving charges. According to the basic physics right hand rule the charged carriers accumulate at the edges of the sample orthogonal to their original direction, creating a measurable voltage. Depending on the direction of the B-field and the sign of the voltage (V_H) the carrier type is easily extracted (see Figure 2.13).

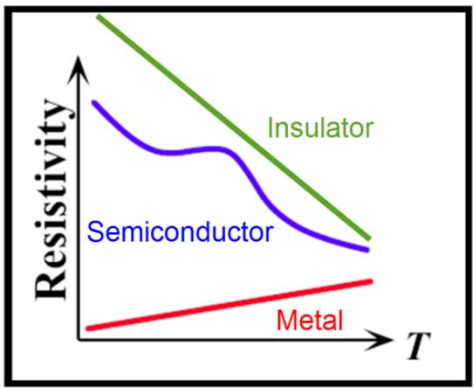

Figure 2.11. Generic plot of the basic shapes of resistance vs temperature for metals, semiconductors, and insulators.[6]

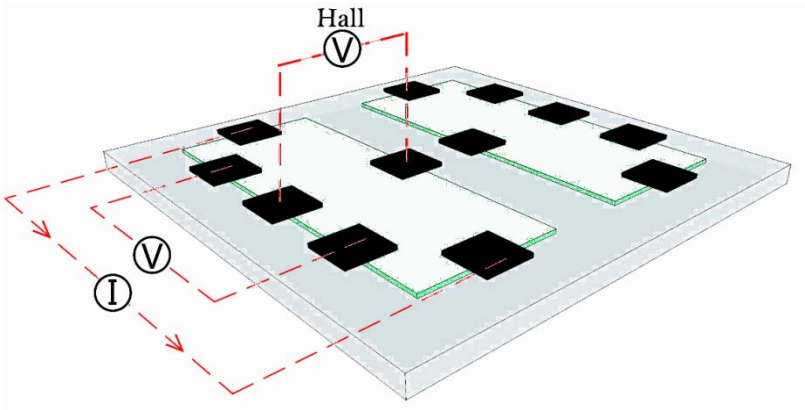

Figure 2.12. Schematic of devices created, showing both the four probe resistance and Hall probe configurations.

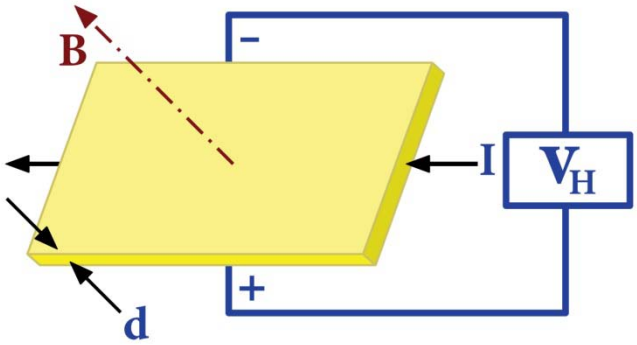

Figure 2.13. A representation of Hall measurement configuration, showing current flow direction, with a B-field normal to the surface, and the resulting voltage that develops.[6]

Furthermore by taking Hall measurements at many temperatures the 2- dimensional sheet carrier concentration n (cm^{-2}), and the mobility μ_H ($cm^2 V^{-1} s^{-1}$) can be calculated, by the following Equations 2.2 and 2.3, respectively:

$$n = \frac{B\,I}{V_H\,e} \tag{2.2}$$

In Equation 2.2, B and I represent magnetic field and the current, respectively, e is the charge of an electron.

$$\mu_H = \frac{1}{n\,e\,\rho} \tag{2.3}$$

In Equation 2.3, ρ represents the resistivity. With the data attained from these equations the number of extrinsic carriers and intrinsic carriers can be found at a given temperature. Also the activation energy of thermal carriers and can be found by plotting ln (n) vs. 1/T as seen in Figure 2.14.

2.7.3 Thermoelectric Power Measurements

Thermoelectric power is voltage difference that develops across a material due to a temperature difference. A schematic illustrating the basic effect can be seen in Figure 2.15. In order to measure the thermoelectric power of the 2DEGs created it was very important to thermally isolate the hot and cold sides of the substrate from each other. Equally important was the need to measure the real time film temperature. This process is

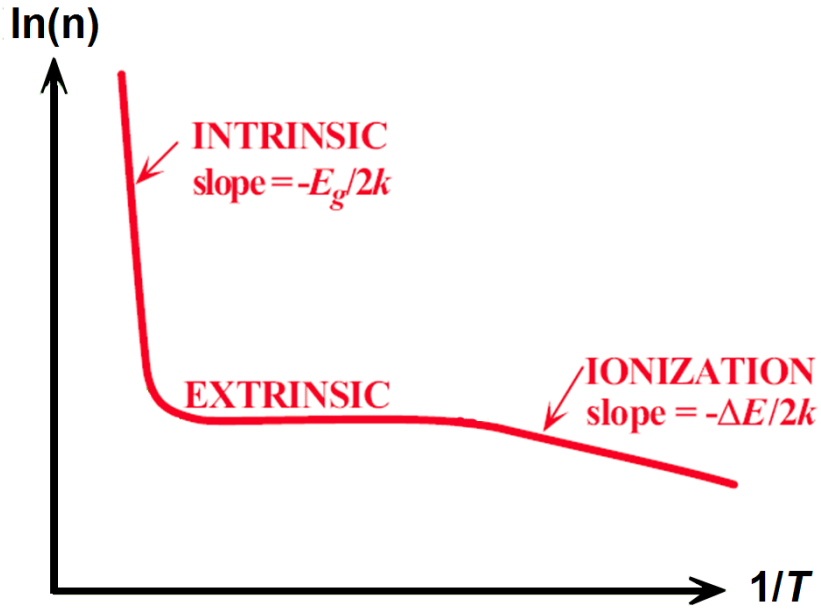

Figure 2.14. A generic plot of the natural log of carriers vs. 1/T for an n-type material. Figure adapted by Kasap.[6]

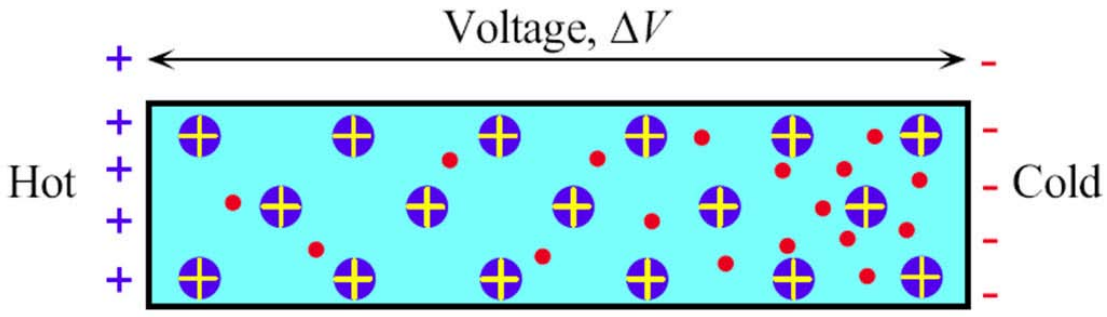

Figure 2.15. An illustration of the thermoelectric effect, where a temperature difference gives rise to the development of a potential (V) across the sample. Figure adapted by Kasap.[6]

outlined and thoroughly detailed in section 2.5.3.

A Lakeshore 352 temperature controller was employed to control both the onboard circuit heater and the internal heater of a Janis 22 cryostat. The temperature controller also recorded the temperatures of both sides of the sample. The voltage that developed across the sample was measured using a Keithley 6514 System Electrometer. The entire measurement process was controlled and automated by a Labview program.

The measurement was carried out by starting at low temperature (10 K) and turning on the on board heater which was on the hot side of the sample. This continued until a delta T in excess of 5 K was reached. At this point the whole system was heated to the new temperature and allowed to reach thermal equilibrium. The process was repeated upto a base temperature of 300 K.

Analysis of the data began by plotting the difference in voltage (ΔV) vs. the difference in temperature (ΔT) over the intended temperature range. The slope of this line yields the value of the Seebeck coefficient (S), this relationship is shown Equation 2.4:

$$S = -\frac{\Delta V}{\Delta T} \tag{2.4}$$

The sign of the Seebeck coefficient indicates the type of carriers present, if electrons are the carriers (n-type) then a negative Seebeck coefficient is found.

Other important thermoelectric parameters are the Figure of Merit (Z) and the unit-less parameter known as ZT. These two values are the parameters used to compare the efficiency of different thermoelectric materials. Equation 2.5 demonstrates how the parameters Z and thus ZT are calculated.

$$Z = \frac{\sigma S^2}{k} \tag{2.5}$$

Here σ and k represent the resistivity and the thermal conductivity of the material. The parameter ZT is calculated by multiplying Z by the absolute temperature.

2.8 References

1. Ohtomo, A.; Hwang, H. Y., A high-mobility electron gas at the LaAlO3/SrTiO3 heterointerface. *Nature* **2004,** *427* (6973), 423-426.

2. Pauli, S. A.; Willmott, P. R., Conducting interfaces between polar and non-polar insulating perovskites. *Journal of Physics-Condensed Matter* **2008,** *20* (26).

3. Xu, Y., *Ferroelectric materials and their applications*. North-Holland ; Sole distributors for the USA and Canada, Elsevier Science Pub. Co.: Amsterdam ; New York, New York, 1991; p xiv, 391 p.

4. Yang, R.; Shen, S. Y.; Wang, C. B.; Shen, Q.; Zhang, L. M., Pulsed laser deposition of stoichiometric KNbO3 films on Si (100). *Thin Solid Films* **2008,** *516* (23), 8559-8563.

5. Singh, R. K.; Narayan, J., Pulsed-laser evaporation technique for deposition of thin films: Physics and theoretical model. *Physical Review B* **1990,** *41* (13), 8843-8859.

6. Kasap, S. O.; Kasap, S. O., *Principles of electronic materials and devices*. Boston : McGraw-Hill: Boston, 2002.

CHAPTER 3

THE FORMATION AND STUDY OF LAO/STO 2DEGs

3.1 Abstract

Oxide based materials are one of the most investigated materials currently. The oxides have traditionally served the electronics industry as simple insulating layers for integrated circuits. Oxides are now being intensely studied as the active primary device. Much of this oxide based research is centered on perovskite materials containing a multivalent transitional metal. These materials are strongly correlated electron systems (SCES), where small changes can affect both the spin and orbit of the outer electrons. One of the most intriguing and most explored such system is the thin film heterostructure of $LaAlO_3$ deposited on a $SrTiO_3$ substrate. Ohtoma et al. have recently shown this system to produce a metallically conductive interface.[1] This 2-dimensional electron gas has displayed many interesting properties including high mobility, large carrier densities, low resistance, and low T superconductivity/magnetic effects. The mechanisms involved in these phenomena are not fully understood. An in-depth study of the LAO/STO 2DEG was conducted in this study; all films were grown via PLD. Carrier densities as high as ~5 x 10^{16} cm^{-2} at room temperature, with the largest mobility in excess of 5000 $cm^2 V^{-1} s^{-1}$ at 10 K. The need for an atomically abrupt and terraced interface is also investigated.

3.2 Background and Introduction

The use of oxide materials for electronic and semiconducting applications has recently made a dramatic shift. Oxides have typically been used as passive insulators for integrated Si based circuits. Currently the oxide materials are being used and researched as active functioning devices. Several examples include indium tin oxide used for display panels and organic type solar cells (DSSC's) and zinc oxide in thin film transistors and light emitting diodes.

Oxide based research is still in its infancy, and differs greatly from the traditional semiconductor field. Semiconductors typically exhibit a single functionality which is easily controlled and very well understood. Oxide materials, however, exhibit strong coupling between magnetic, ferroelectric, superconductivity, semiconductivity and metallic conduction.[1-3] This multifunctionality of the oxide materials has spawned worldwide in-depth research.[3] A well known example of this effect is the electro-mechanical coupling of piezoelectric materials such as lead zirconate titanate (PZT). Dramatic shifts in oxide properties can be induced by very subtle changes such as impurities, lattice strain, and environmental changes. This sensitivity of the oxides is both fascinating but has presented many challenges in reproduction and the understanding of the mechanisms involved.

One of the most studied and intriguing oxide groups is the perovskite family. Perovskites have the general formula of ABO_3. The crystal structure is a mixture of both face and body centered cubic, where the A site exists at the corners, oxygen on the faces, and the B site resides in the central octahedron. The structure can be thought of as alternating atomic layers of AO and BO_2. Of particular interest are the perovskites

containing a multivalent transition metal at either the A or B site. The resulting material can be neutral between layers when the oxidation states are $A^{2+}B^{4-}O^{2-}{}_3$, or possess a dipole (polarity) between layers with the $A^{3+}B^{3-}O^{-2}{}_3$ states. The perovskite structure can be easily doped at both the A and B sites and will maintain its structure despite many oxygen vacancies. The lattice parameters of the perovskite family are very close, usually around 4Å. This similarity enables the creation of 'epitaxial' heterostructures with relative ease.

One such heterostructure was shown by Ohtomo et al. to create an all oxide 2-dimensional electron gas (2DEG) at the hetero-interface of two band insulators, lanthanum aluminum oxide (LAO) thin film on strontium titanate (STO) substrate.[4] The resulting interfaces exhibit metallic conduction with low resistance. This was accomplished via pulsed laser deposition (PLD) on an all Ti-terminated STO substrate (001) with varying oxygen partial pressures from 10^{-2}-10^{-6} torr. They reported high mobility of 10^4 cm^2 V^{-1} s^{-1}, despite a large sheet carrier density of 10^{14}-10^{16} cm^{-2}. In contrast an all Sr-terminated surface yields an electrically insulating surface.

The mechanism for the formation of the 2DEG is a hotly debated subject, and is, of yet, undetermined. One of the leading theories is that of the polar catastrophe, in which the polar LAO film has a dipole present between the alternating layers, and the STO is neutral. The existence of the interfacial dipole would create a divergence in the potential and create a large energetically unfavorable surface charge on the LAO.[5] In the n-type case (Ti terminated), to avoid this it is thought that electronic reconstruction occurs. Where every other Ti atom at the interface would switch from a 4+ state to a 3+ state, thus donating ½ an electron charge to the interface (Figure 3.1 a, c). For the p-type

interface (Sr terminated) the avoidance can only be caused by an atomic reconstruction, where oxygen vacancies form producing ½ hole charge to the interface (Figure 3.1 b, d).[6] According to the electronic reconstruction theory, ½ an electron charge should yield ~3.3 x 10^{13} carriers per cm^2. Many groups, even Ohtomo et al., found carrier concentrations well above this level (10^{14} -10^{16}).[4] The high carrier concentrations observed suggest that there is more to the conduction at the interface.

An undeniable addition to the conductance of the 2DEG, is that of oxygen deficiency. The effect of oxygen vacancies has been proven to directly affect the resistance and carrier concentration of the 2DEG.[7] This has been shown by either varying the oxygen partial pressure during deposition, or by annealing in an oxygen environment at high temperatures. Both of these methods indicate that oxygen vacancies do indeed increase the conductance of the n-type 2DEG.[8] High oxygen partial pressure, either during deposition or annealing, has even been shown to produce an insulating n-type interface.[8] This interesting research suggests that oxygen vacancies could be the dominant carrier.

More complications in the 2DEG theoretical explanations are the assumptions and idealizations that are made. A generally accepted requirement for 2DEG formation is that of an atomically abrupt and sharp interface.[4, 9, 10, 11] Theoretical and experimental work tends to assume this type of ideal interface. Furthermore an STO terraced surface structure is most commonly prepared and much theoretical work assumes this surface exists.[2] Interdiffusion of cations is also most often ignored, although it has been proven to occur by several groups.[8] It is well known that lanthanum substitution at strontium sites (La_{Sr}) is a donor, as $Sr_{1-x}La_xTiO_3$ is a known conductor. Assumptions are also made in

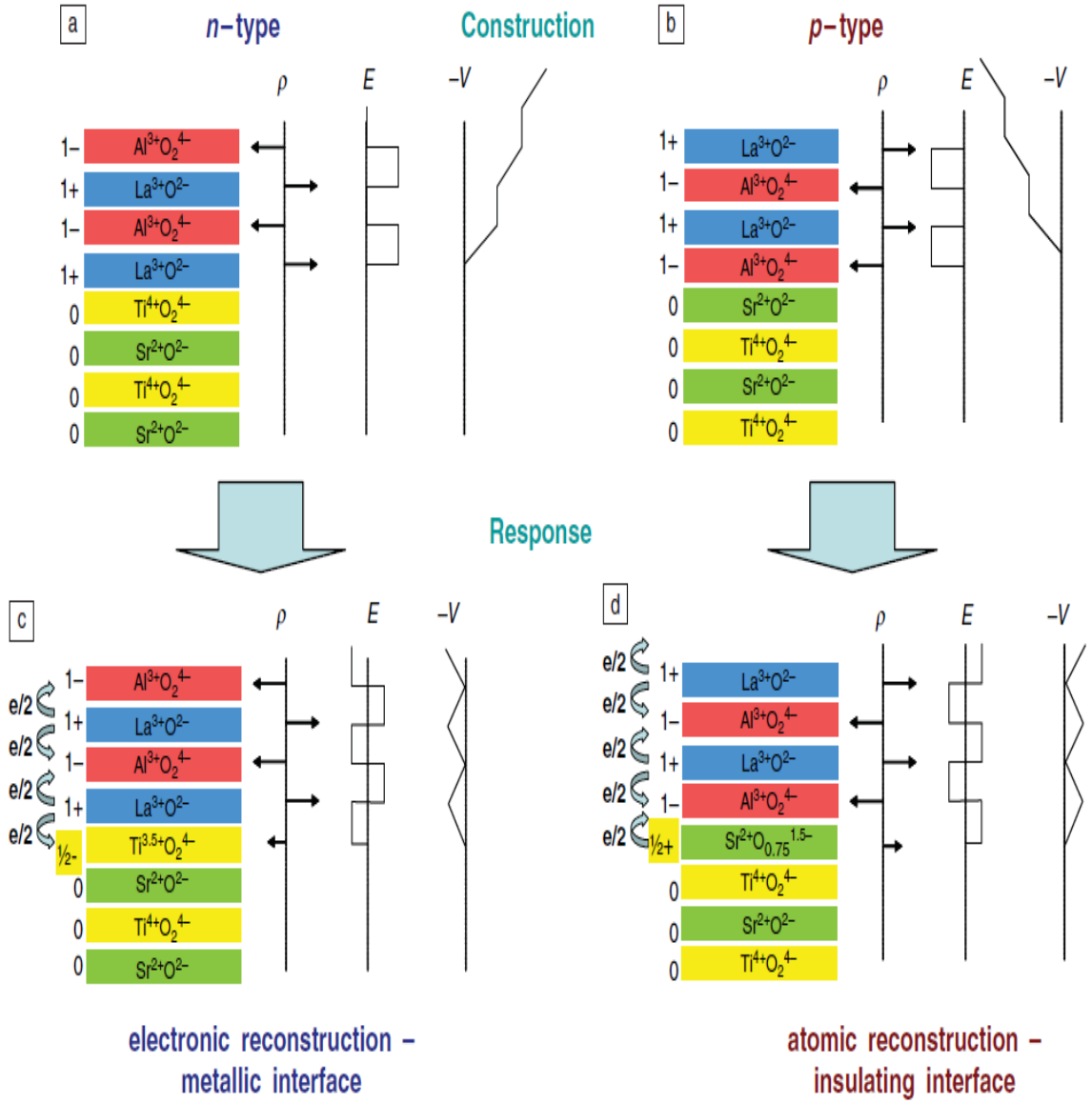

Figure 3.1 Schematic showing the avoidance of a polar catastrophe for both the n-type (a, c), and the p-type (b, d) interfaces. The ½- sheet carrier concentration is roughly equal to 3.3 x 10^{13}. [6]

most of the theoretical work, which should not be overlooked. One assumption is that the electron-electron and ion-ion interactions are insignificant under most circumstances. However, these interactions are very pronounced in strongly correlated electron systems (SCES). Transition metal oxides are a member of the SCES. Due to all of these competing factors the mechanisms responsible for the 2DEG formation are not likely to be fully explained or agreed upon in the oxide community anytime soon. The authors have thus joined in the world wide effort in an attempt to further understand the mechanisms responsible.

3.3 Experimental Procedure

Following the work done by Ohtomo et al., a six-probe Hall geometry was chosen for the construction and testing of the LAO/STO 2DEGs. This was accomplished using a two-step contact shadow mask procedure utilizing a theta z mask aligner. The device design and the testing fixture circuit schematic can be seen in Figure 3.2. In order to ensure interfacial contact, an overlapping contact design was chosen. This design enabled two methods for interfacial contact. The first method being direct edge contact and second is the diffusion of Pt through the ultrathin films. Others have reported the need for laser/thermal annealing of the contacts, and Ar ion etching to the interface. The authors chose a two-prong method for interfacial contact. The platinum overlaps the film and substrate continuously for direct edge contact (Figure 3.2). Furthermore the author's experience has shown that Pt will make contact with the substrate surface through the film (even if this is not desired) directly with higher fluence PLD without the need for contact annealing. The films were deposited via PLD using a single crystal LAO target,

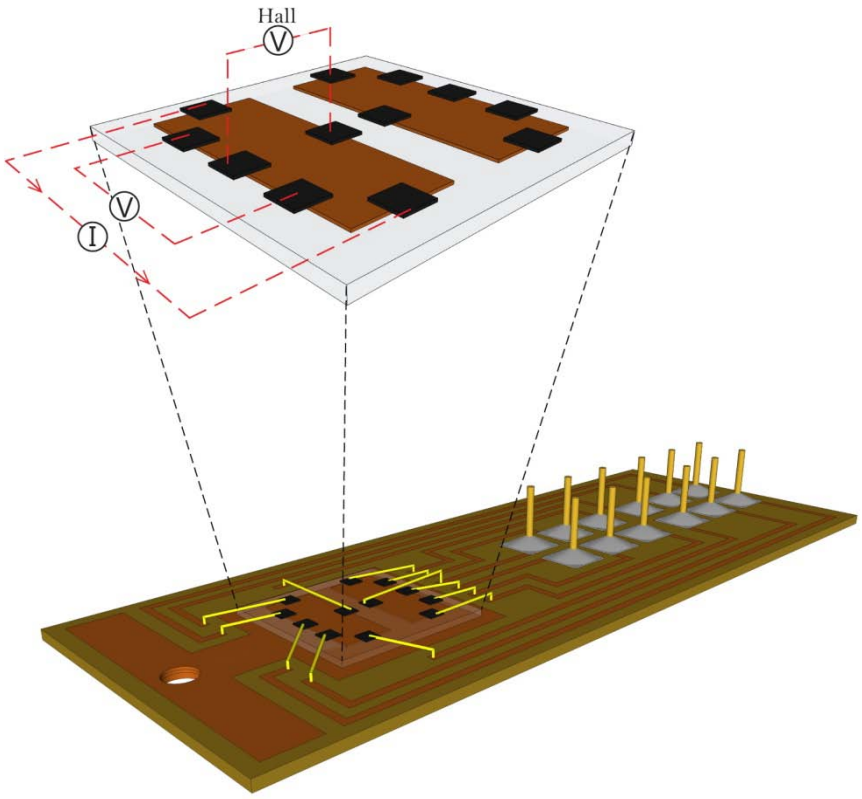

Figure 3.2 Schematic of the oxide devices produced from the two stage PLD *in situ* mask process (top). Schematic of the testing fixture used to electrically analyze the 2DEGs (bottom).

followed by the deposition of Pt contacts without breaking vacuum. The laser fluences used were, 3.5 J cm^{-2} on the LAO target, and 5.5 J cm^{-2} for the Pt. All films were deposited at 650° C, with an oxygen partial pressure of 10^{-6} torr. PCB testing circuits were designed to hold the devices securely and enable the ability for wire bonding (Figure 3.2). The testing circuits were designed to fit the stage of a liquid helium closed cycle cryostat. A direct copper thermal contact was created between the top and bottom of the PCB circuit directly below the substrate. The substrate and the testing board were held in place using thermal grease, thus ensuring temperature accuracy during measurements.

The substrates used were single crystal STO (001). All single crystals were purchased through MTI xtl. The STO underwent an HF etching process to preferentially remove Sr, leaving a Ti terminated surface. LAO film thicknesses of 200, 100, 50, 25, 10, 5nm were deposited. All of the films received the same film thickness of Pt contacts which was 20nm. A control film of Ti terminated STO with only Pt contacts deposited was produced under the same conditions as the other LAO films (O_2 pressure and temperature). Film thickness and surface roughness were confirmed with profilometry (Tencor P-10) and AFM (Bruker Dimension ICON-PT). The crystallinity of the films was analyzed using XRD (Philips X'pert diffractometer). Electrical analysis included sheet resistance vs. temperature, and Hall measurements both performed in the temperature range of 300-10 K. From these data, mobility, carrier concentrations and activation energies were calculated.

3.4 Results and Discussion

3.4.1 Structural Characterization

Film thicknesses were confirmed via optical profilometry, and indicated that the actual thickness was within 2-5% of the targeted values. Atomic force microscopy found the RMS roughness of the STO substrate and LAO film to be 3 and 4.6 Å, respectively. The RMS values indicate a smooth and even film distribution, with roughness difference from the substrate of less than ½ of a unit cell. As can be seen in Figure 3.3, a non-terraced surface is revealed which indicates the lack of an atomically abrupt and sharp interface as previously stated, thus providing further evidence that quantum confinement at the interface is not the only conduction mechanism.

XRD analysis revealed only STO peaks of the [100] family, as to be expected for the crystallographic direction of the substrate. No LAO peaks were observed, indicating an “epitaxial" thin-film. The XRD scan can be seen in Figure 3.4. Although phi theta scans were not performed to prove heteroepitaxy, the film can be easily assumed epitaxial as the lattice parameters of the film and substrate are very similar and the films deposited were ultrathin, as the thinner the film the interfacial bonding energy is sufficient to prevent dislocations.[12]

3.4.2 Electrical Characterization

Resistance versus temperature measurements were taken for all film thicknesses and for the control. The control STO which as previously stated, had Pt deposited under the same conditions as the LAO films. The control STO resistance was immeasurable (<< 200 GΩ). The resistance of the thicker LAO films (200 and 100 nm) was also

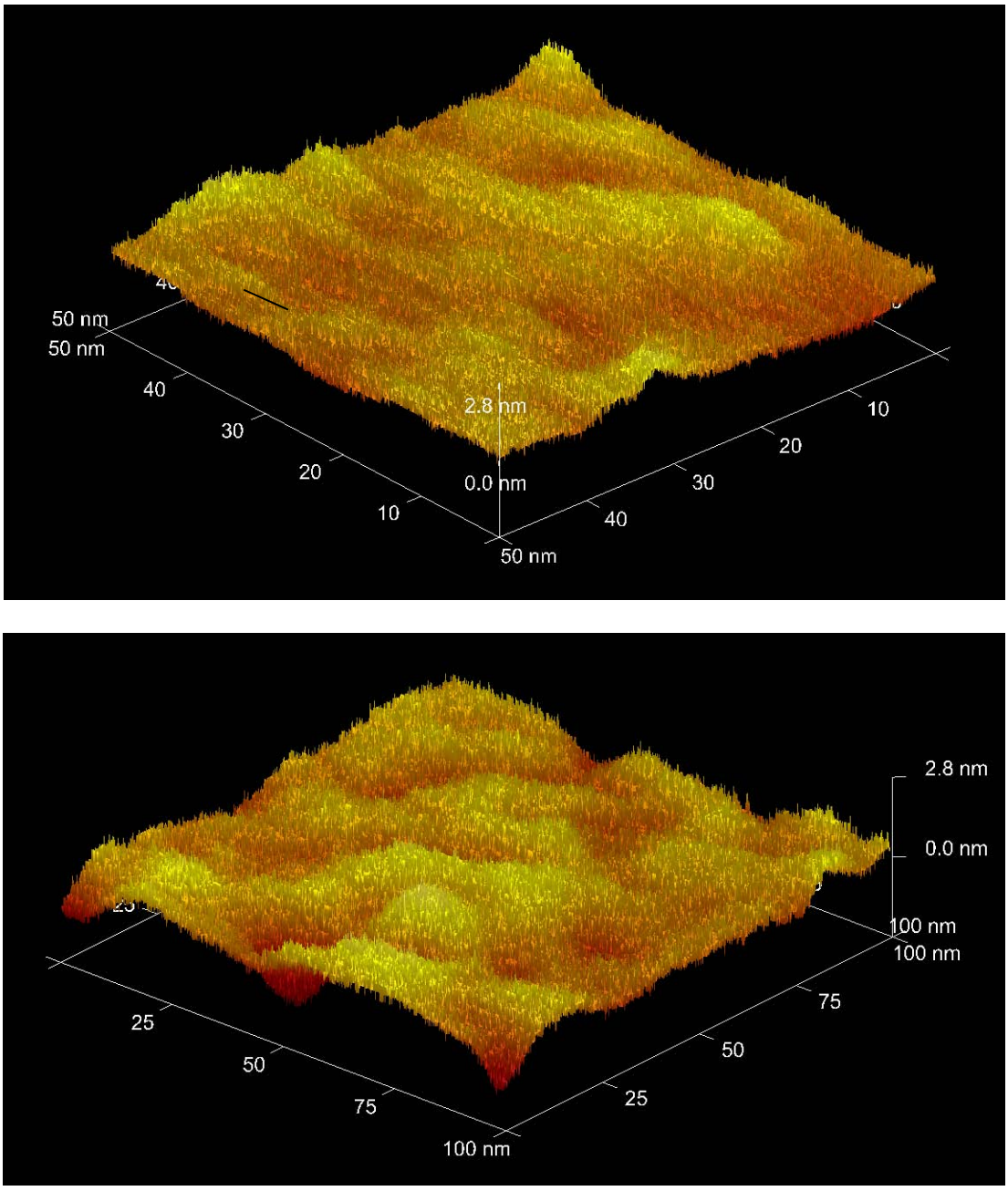

Figure 3.3 Atomic force microscopy (AFM) images of the STO substrate (Top), and the LAO film on STO (Bottom). The RMS roughness values found were 3 Å and 4.6 Å, respectively.

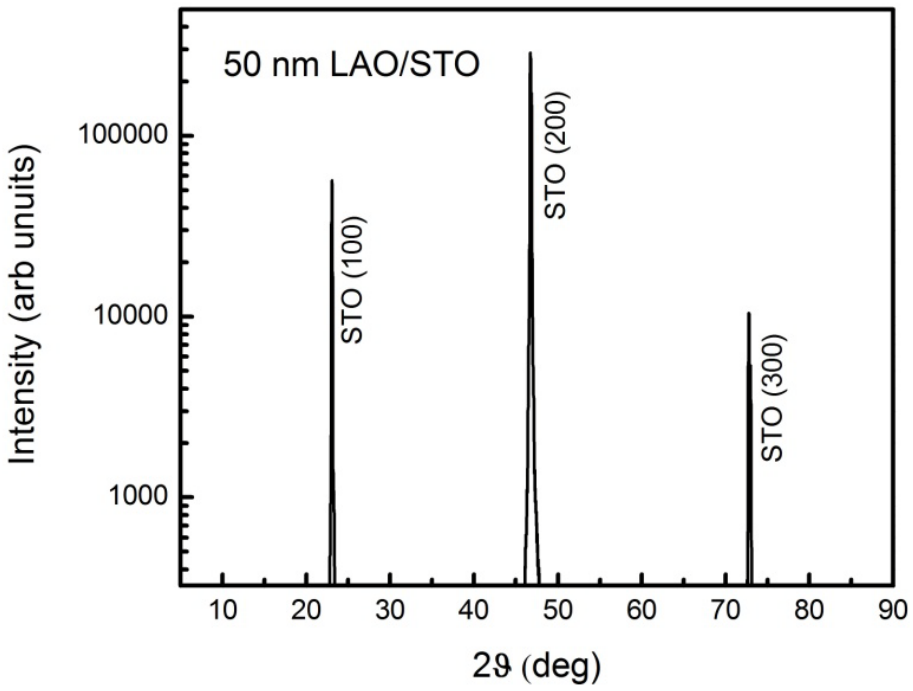

Figure 3.4 X-ray diffraction (XRD) scan of the 50 nm LAO film deposited on STO. The scan only reveals strong STO peaks of the [100] family, indicating epitaxial growth as no LAO peaks are present.

immeasurable. However, the other thin films (50, 25, 10 and 5nm) exhibited metallic-like conduction with low resistance.

The sheet resistance vs. versus temperature is presented in Figure 3.5. The graphs reveal an interesting trend that goes against the general belief that the thinner the film is the lower the resistance will be. This is demonstrated by the fact that the 50 nm thick film is three to four orders of magnitude less resistive than the thinnest film of 5 nm at room temperature. At 10 K the 50 nm film drops in resistance to 30 mΩ, while the 5 nm film drops to 337 Ω.

Hall measurements were taken on all samples in the temperature range and magnetic field strength of, 300 K to 10 K, and ± 5 kG, respectively. An example of Hall voltage vs. Magnetic field of the same sample at high and low temperature values can be seen in Figure 3.6. From the Hall data, the sheet carrier concentration n_H (cm^{-2}) and the mobility μ_H ($cm^2\ V^{-1}\ s^{-1}$) was extracted. A large number of carrier concentrations were found, with the largest being ~4 x 10^{16} cm^{-2} in the 50 nm thick film at room temperature.

At the same temperature, the thinnest film (5 nm) had lower carrier concentrations which were found to be around 2.2 x 10^{14} cm^{-2}. Several comparisons of carrier concentrations can be seen in Figures 3.7 and 3.9, while the mobilities are compared in Figures 3.8 and 3.10. In Figure 3.9, it can be seen that both the 5 and 10 nm LAO films have very comparable carrier concentration values. From Arrhenius plots of the carrier concentrations the number of extrinsic carriers and the activation energies (E_a) were calculated. The thermal activation energies were found to be very small in the 10 meV range. This low activation energy indicates the presence of very shallow donars at or near the interface.

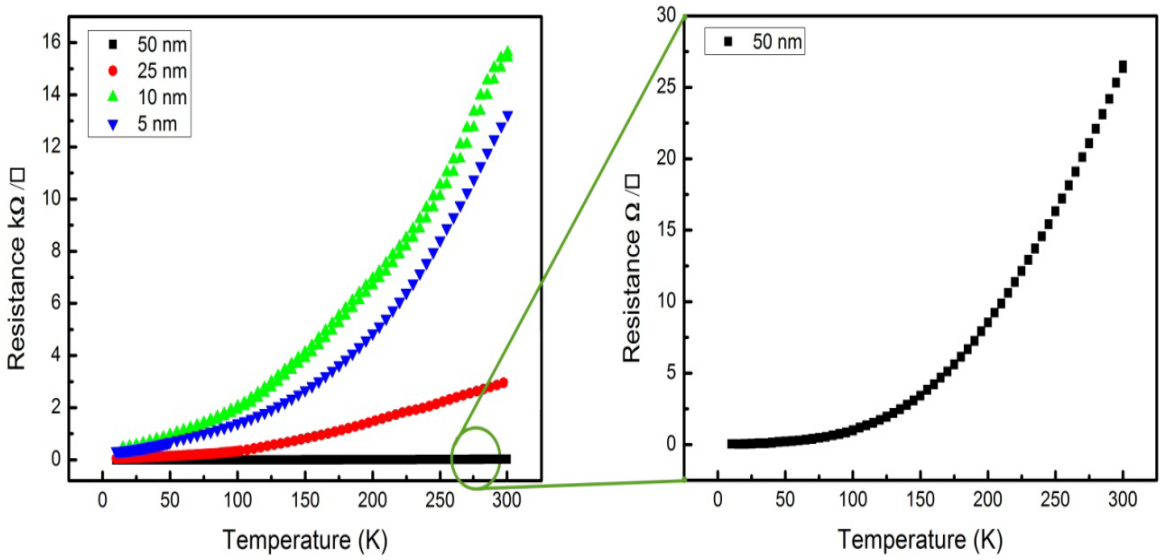

Figure 3.5 Sheet resistance vs. temperature, data collected from 300K to 10K. The graph on the left shows all films plotted together with a y-axis unit of kΩ. The 50 nm film R vs. T is plotted individually on the right with a y-axis unit of Ω.

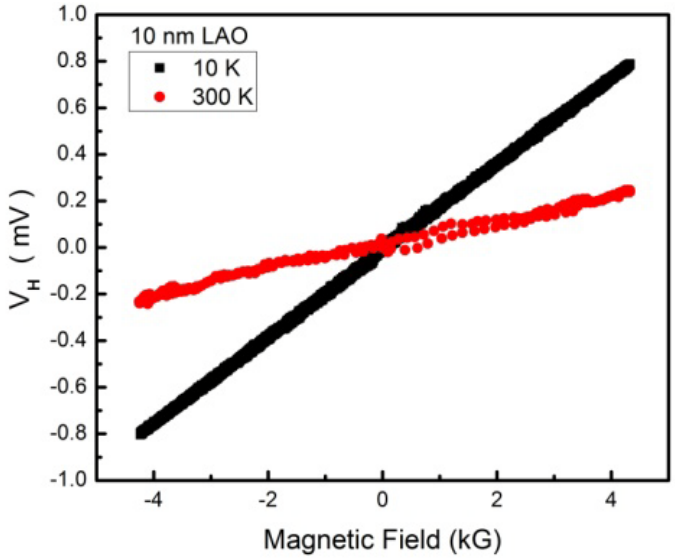

Figure 3.6 Hall measurements taken on the 10 nm LAO/STO devices, showing only the plots collected at the temperature extremes. Raw data are plotted, indicating the clarity of the measurements.

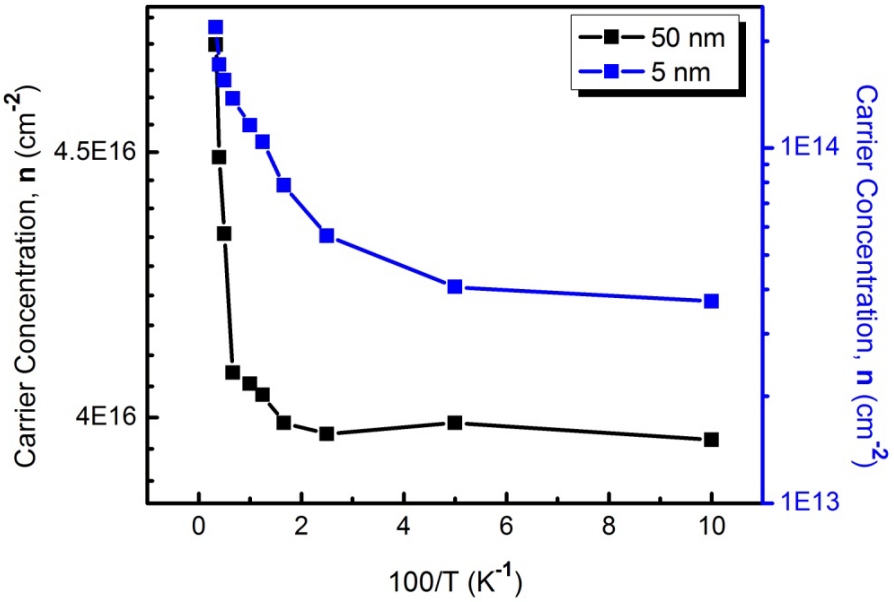

Figure 3.7 Double Y-axis plot of carrier log(n) vs. 1/T, of the 50 and 5nm LAO films, illustrating the marked difference between the carrier numbers.

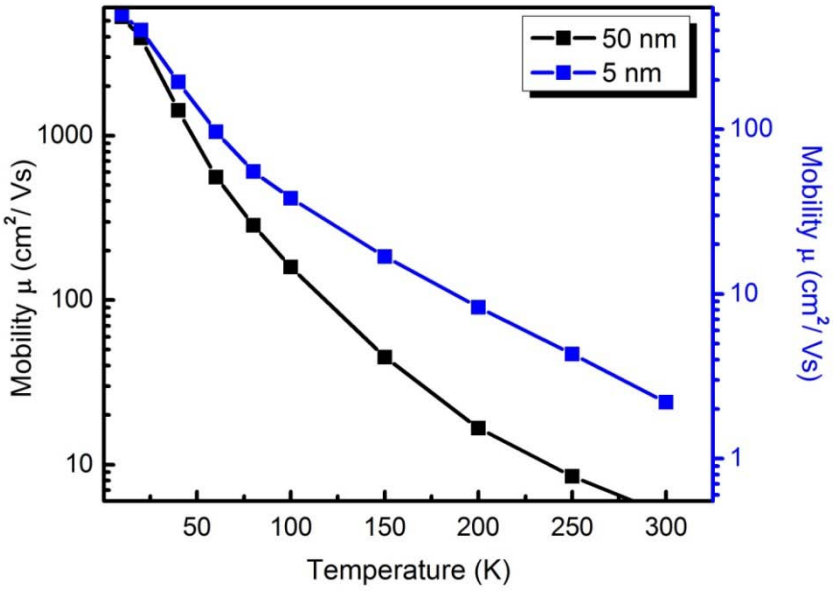

Figure 3.8 Double Y-axis plot of Hall mobility vs. temperature of the 50 and 5nm LAO films, demonstrating the higher mobility of the 50nm film, despite the higher number of carriers.

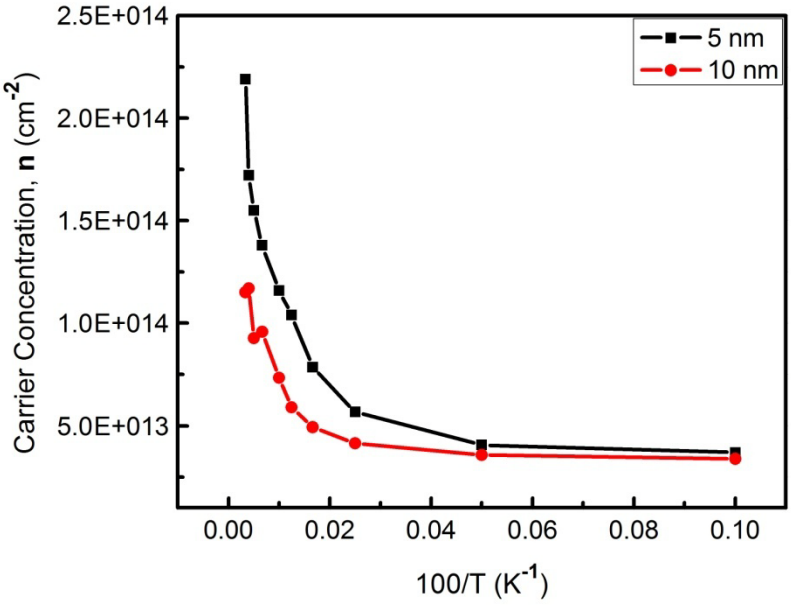

Figure 3.9 Plot of carrier concentration log (n) vs. 1/T, of the 10 and 5nm LAO films.

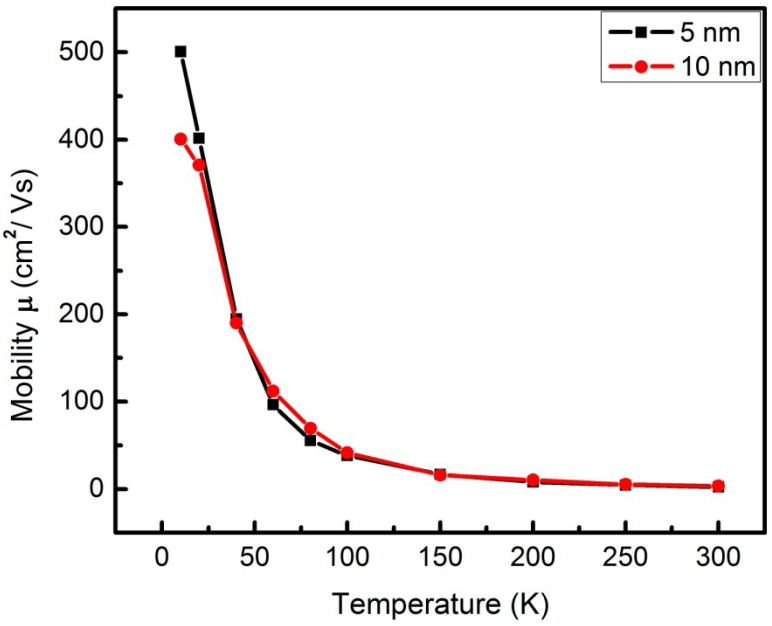

Figure 3.10 Plot of the Hall mobility vs. temperature of the 10 and 5nm LAO films.

The mobility calculations followed similar trends as the sheet resistance and carrier concentration, where the 50 nm LAO film had the highest mobility. This mobility ranged from 5300 at 10K, and down to 5 $cm^2 V^{-1} s^{-1}$ at 300K. Compared to the 5 nm thin film had a range of 500 to 2 $cm^2 V^{-1} s^{-1}$ at the same temperatures. The comparison of the widely varied mobilities of the 50 and 5 nm LAO films can be seen in Figure 3.8, while the similar mobilities of the 10 and 5 nm LAO films can be seen in Figure 3.10.

3.5 Conclusions

It has been shown and suggested by multiple groups that the most successful 2DEGs are produced with an LAO film thickness of about 2-10 nm.[2, 13, 14] Although the data presented herein suggest optimal thickness to be around 50 nm. The 5 nm thin film performed orders of magnitude worse than the 50 nm film as revealed in Table 3.1. The trend of the sheet resistance further confirms that the 50 nm film out performs the thinner films. Furthermore this study has shown that films in excess of 100 nm cease to behave metallically (Section 3.3).

The experimental discussions and first principle calculations have also indicated that an idealized atomically abrupt and sharp interface is necessary.[6, 8, 14, 15] An atomically terraced substrate surface is also imaged and described as being necessary to produce functional oxide 2DEGs.[6] The substrate preparation that is typically reported indicates the need for high temperature/oxygen pressure during annealing after the HF etching process, which produces this terraced structure. However this annealing procedure was not followed in this study. The STO preparation consisted only of the preferential HF etching followed directly by the deposition of LAO. As was shown in the AFM images

in Figure 3.3, neither an abrupt, or terraced structure was formed, although the electrical transport properties recorded are on the same order of magnitude as most of the reported high end values with this interface (Table 3.1). This demonstrates that the assumption and preparation of an atomically abrupt interface is not required.

These results indicate that the LAO/STO 2DEG formation cannot simply be explained by the polar catastrophe theory, as this theory assumes an abrupt interface resulting in a ½ electron charge[4] (this charge is roughly equal to 3.3×10^{13} cm^{-2}). As this study has shown the carrier concentrations are much higher than the predicted ½ electron charge. This has also been confirmed by many other groups, including Ohtomo himself.[4]

It is well accepted that oxygen vacancies play an important role in the addition of the number of carriers. Furthermore, oxygen vacancies will not be confined to the surface but will diffuse well into the substrate. This could indicate that the conduction is not simply a 2-dimensional pathway. In support of a possible 3-dimensional conductor is cation interdiffusion, which cannot either be ignored, or assumed to only occur at the interface alone. The diffusion process for vacancies and ions is exponentially proportional to temperature, thus leading the author to believe that the phenomenon is neither a 2DEG nor a quasi-2DEG, but a 3-dimensional conduction channel of which the thickness is unknown and likely varies.

In conclusion, the mechanisms involved in the conduction of the LAO/STO heterostructure are more complicated than previously believed. This work proves that the assumptions and idealizations of the perfect interface are not accurate. Some further work that is suggested is the use of a substrate with a much higher RMS surface roughness. This could not only support the work performed herein, but it may also find the thickness

of the third dimension of the conduction pathway, if one exists. The author intends to find the contribution that oxygen vacancies have on the carrier concentration. This may be accomplished by depositing STO on STO under the same LAO conditions, via PLD. The resistance of the resulting film should indicate which of the two most accepted mechanisms is dominant.

Subtle changes are well known to have profound effects on the properties of the oxide perovskite family, thus creating a vast difference in the 2DEG performances between the competing laboratories. This only adds fuel to the fiery debate over the mechanisms involved. As oxide based electronics is still in its infancy, it is doubtful that the driving forces will be fully explained or agreed upon in the near future.

The work contained herein does not claim to have solved any portion of the mechanisms responsible for the 2DEG formation; the contrary is more correct. The results attained seem to point to an even more complex system than what was previously assumed.

Table 3.1. A summary table of the electrical characterization results including the number and types of carriers, Hall mobility, sheet resistance, and activation energy.

Property	Units	50 nm	10 nm	5 nm
Extrinsic ~300 K	Carriers/cm^2	4.72E+16	3.88E+13	3.48E+13
Intrinsic ~10K	Carriers/cm^2	3.97E+16	1.15E+14	2.19E+14
Ea Activation Energy	meV	10.14	11.36	7.18
Ea Standard Error	%	2.58	5.36	4.67
Hall Mobility ~300 K	cm^2/Vs	5.1	3.5	2.2
Hall Mobility ~10K	cm^2/Vs	5254.4	400.5	500.6
Sheet Resistance ~300 K	Ω/□	26.4	15620	13230
Sheet Resistance ~10 K	Ω/□	0.03	460	337

3.6 References

1. Hwang, H. Y., Atomic control of the electron structure at complex oxide heterointerfaces. *Mrs Bulletin* **2006,** *31* (1), 28-35.

2. Pauli, S. A.; Willmott, P. R., Conducting interfaces between polar and non-polar insulating perovskites. *Journal of Physics-Condensed Matter* **2008,** *20* (26).

3. Ariando; Wang, X.; Baskaran, G.; Liu, Z. Q.; Huijben, J.; Yi, J. B.; Annadi, A.; Barman, A. R.; Rusydi, A.; Dhar, S.; Feng, Y. P.; Ding, J.; Hilgenkamp, H.; Venkatesan, T., Electronic phase separation at the LaAlO3/SrTiO3 interface. *Nature Communications* **2011,** *2* (1).

4. Ohtomo, A.; Hwang, H. Y., A high-mobility electron gas at the LaAlO3/SrTiO3 heterointerface. *Nature* **2004,** *427* (6973), 423-426.

5. Caviglia, A. D.; Gariglio, S.; Reyren, N.; Jaccard, D.; Schneider, T.; Gabay, M.; Thiel, S.; Hammerl, G.; Mannhart, J.; Triscone, J. M., Electric field control of the LaAlO3/SrTiO3 interface ground state. *Nature* **2008,** *456* (7222), 624-627.

6. Mannhart, J.; Blank, D. H. A.; Hwang, H. Y.; Millis, A. J.; Triscone, J. M., Two-dimensional electron gases at oxide interfaces. *MRS Bulletin* **2008,** *33* (11), 1027-1034.

7. Eckstein, J. N., Oxide interfaces - Watch out for the lack of oxygen. *Nature Materials* **2007,** *6* (7), 473-474.

8. Chambers, S. A., Understanding the mechanism of conductivity at the LaAlO 3/SrTiO3(001) interface. *Surface Science* **2011,** *605* (13-14), 1133-1140.

9. Gariglio, S.; Reyren, N.; Caviglia, A. D.; Triscone, J. M., Superconductivity at the LaAlO3/SrTiO3 interface. *Journal of Physics Condensed Matter* **2009,** *21* (16).

10. Reyren, N.; Thiel, S.; Caviglia, A. D.; Kourkoutis, L. F.; Hammerl, G.; Richter, C.; Schneider, C. W.; Kopp, T.; Ruetschi, A. S.; Jaccard, D.; Gabay, M.; Muller, D. A.; Triscone, J. M.; Mannhart, J., Superconducting interfaces between insulating oxides. *Science* **2007,** *317* (5842), 1196-1199.

11. Guisinger, N. P.; Santos, T. S.; Guest, J. R.; Chien, T. Y.; Bhattacharya, A.; Freeland, J. W.; Bode, M., Nanometer-scale striped surface terminations on fractured SrTiO3 surfaces. *ACS Nano* **2009,** *3* (12), 4132-4136.

12. Singh, R. K.; Narayan, J., Pulsed-laser evaporation technique for deposition of thin films: Physics and theoretical model. *Physical Review B* **1990,** *41* (13), 8843-8859.

13. Willmott, P. R.; Pauli, S. A.; Herger, R.; Schleputz, C. M.; Martoccia, D.; Patterson, B. D.; Delley, B.; Clarke, R.; Kumah, D.; Cionca, C.; Yacoby, Y., Structural basis for the conducting interface between LaAlO3 and SrTiO3. *Physical Review Letters* **2007,** *99*.

14. Park, J. W.; Bogorin, D. F.; Cen, C.; Felker, D. A.; Zhang, Y.; Nelson, C. T.; Bark, C. W.; Folkman, C. M.; Pan, X. Q.; Rzchowski, M. S.; Levy, J.; Eom, C. B., Creation of a two-dimensional electron gas at an oxide interface on silicon. *Nature Communications* **2010,** *1*, 94.

15. Nakagawa, N.; Hwang, H. Y.; Muller, D. A., Why some interfaces cannot be sharp. *Nature Materials* **2006,** *5* (3), 204-209.

CHAPTER 4

THERMOELECTRIC POTENTIAL OF LAO/STO 2DEGs

4.1 Abstract

For well known reasons there has been worldwide thrust into research focused on alternative energy. The desired materials need to be renewable, efficient, abundant, and environmentally friendly (both in production and use).

More than 30% of the total energy produced in the world is wasted in the form of heat. This is a staggering number; the world produces 5.33 x 10^20 Joules annually, with 1.6 x 10^20 Joules wasted as thermal energy (US-DOE). There is class of materials that possesses the unique ability to harness this waste energy and transform it into useable electricity, thermoelectric materials.

Thermoelectric power generation (TEP) is based on the Peltier-Seebeck effect, where a voltage develops across a material whenever a temperature difference exists, and vice versa. This phenomenon has been exploited for decades, mainly for refrigeration. Some automobiles have been utilizing TEPs on their exhaust pipes; this is an exciting step forward. However the current workhorse materials for TEP applications (the alloys of: Bi_2Te_3, Bi_2Se_3, and Pb_2Te_3) are environmentally toxic, both during manufacture, and in high temperature applications. One of the major needs is to harness the energy from

the biggest energy wasters, the power plants. This presents the need to find efficient material systems that can withstand high temperatures.

Low-dimensional material systems have been suggested as great TEP candidates.[1] Recently several groups have had success with low-dimensional systems, namely 2-dimensional electron gases, using an STO/Nb:STO superlattice structures.[2] Ohta et al. have recently reported a 'Giant Seebeck Coefficient' (S) of 850 μV/K, with this superlattice.

Ohtomo et al. have recently created a new type of 2DEG at the interface of two band insulators LAO/STO.[3] Many groups have followed suit and there has been a fiery debate over the mechanism responsible for the conduction. Regardless of the mechanism these systems possess high mobility (up to 30,000 cm^2/Vs), high carrier concentration, and low resistance.[4] Due to these properties the LAO/STO 2DEGs present great TEP potential.

The plausibility of the LAO/STO system for TEP uses has been thoroughly studied in this report, with great success. We are the first to report the exciting results of this system, with a maximum Seebeck coefficient found to be 780 μV/K. This S value is for a single layered film, which should be considered when comparing to the superlattice results obtained from Ohta.[2]

4.2 Introduction

One of the most urgent problems facing society today is the energy crisis. As the burning of fossil fuels is harmful for the environment and the finite amount is quickly

depleting. Hence worldwide searches for alternative, clean, and the harnessing of waste energy.

Energy harvesting is the topic of this report, particularly the use of thermoelectric power (TEP) generation. The progress of high performance materials for TEP use has advanced dramatically over the past decade. Many material systems have been investigated, some with very promising results.

Currently relatively efficient bulk TEP devices are widely used. However the vast majority is used for refrigeration and not energy harvesting. This is unfortunate as over 30% of the energy produced worldwide is wasted in the form of heat. Great examples are electrical plants, both coal burning and nuclear power plants. They release huge amounts of heat into the atmosphere, but there exists a logistical issue of the high temperature that is released. The workhorse materials for TEP are alloys of Bi_2Te_3 and Pb_2Te_3 (Se is a common additive). One of the problems with these materials is their toxic nature to the environment, mainly during manufacture due to the volatility of the constituents. They also possess a low melting point which makes their use for power plants and foundries not possible. However, great progress has been made in the automobile industry.

The temperature of the standard automobiles engine block and radiator are usually between 100-150º C, while the exhaust system can approach a temperature of 480º C. Several high end car manufacturers have begun to harness this wasted energy by replacing the alternator with TEPs on the exhaust line. This is not only a major step forward for energy harvesting, but it actually increases the horsepower and fuel efficiency of the vehicle. This is accomplished by the reduction of the drag force needed

to rotate the serpentine belt. Hopefully these benefits will convince other car and machinery manufacturers to follow suit.

It has been proposed by several groups that low-dimensional, even quantum confined conduction channels could revolutionize thermoelectric.[5] This has been explained as the theoretically high mobility and the vastly reduced number of scattering centers. Recently several groups with different material systems have shown some exciting TEP results.[5] In 2007 Ohta et al. reported 'Giant Seebeck' coefficient for a super lattice of STO/Nb:STO, with a Seebeck (S) of 850 μV/K.[6] This is truly a high number, as the Bi based workhorse alloy only has an S value of 200-300 μV/K. Many other groups have tried other low-dimensional systems with limited success.

A two-dimensional electron gas (2DEG) residing at the interface of two text book band insulators, lanthanum aluminum oxide (LAO) deposited on Ti terminated strontium titanate was recently discovered by Ohtomo et al.[3] This discovery started a surge of research into the system, specifically into the not understood mechanisms responsible for the conduction pathway. The leading theory is the avoidance of a polar catastrophe by the donation of an electron to the interface. Competing theories include the presence of oxygen vacancies, and the interdiffusion of cations (see section 3.2 and Figure 3.1 for more details). The hotly debated mechanism/s responsible is far from over.

Regardless the cause they possess great TEP potential; with high mobility (<30,000 cm^2/Vs), low resistance, and '*quantum*' confinement. For these reasons the authors have chosen to study the TEP possibilities of this material system. This report is the first to present on the exciting results of the thermoelectric properties of the

LAO/STO 2DEG system which rival the results of Ohta's ground breaking superlattice structures.

4.3 Experimental Procedures

4.3.1 Thin Film Growth

A two-step contact shadow mask procedure via PLD was utilized to make the LAO/STO devices with Pt contacts. In order to ensure interfacial contact, an overlapping contact design was chosen. The authors chose a two-prong method for interfacial contact. The platinum overlaps the film and substrate continuously for direct edge contact (Figure 3.2). Furthermore experience has shown that Pt will make contact with the substrate surface through the film directly with higher laser fluence, without annealing. A single crystal LAO target was used, followed by the Pt contacts without breaking vacuum. In this study 100, 50, and 5 nm thin films of LAO were grown on (100) STO. The laser fluences used for the LAO and Pt were 3.5 and 5.5 J cm^{-2}, respectively. Films were deposited at 650° C, with an oxygen partial pressure of 10^{-6} torr. A control sample was made depositing Pt contacts directly on STO under these conditions.

4.3.2 Testing Circuit Design

PCB testing circuits were created to thermally isolate the two sides of the sample. On-board heaters were placed directly underneath one side of the substrate. This heated side was milled thinner from underneath to prevent any contact with the cold finger. The 'cold' side of the board was built to have a direct thermal contact with the cold finger. This was accomplished with a copper thermal bridge connecting the top and bottom PCB

copper films (see Chapter 2 for more details). Two Si diodes were placed directly on top of the film with thermal grease. Thermal grease was also placed under the substrate and the testing board. Teflon diode caps were milled and used to apply pressure on each diode separately, thus firmly securing the diodes, substrate and testing board to the cryostage. Hence everything possible was done to both thermally isolate the two sides, and ensure great thermal contacts. A detailed schematic of the testing fixtures is shown Figure 4.1.

4.3.3 Characterizations Utilized

Film thickness and surface roughness were investigated using profilometry (Tencor P-10) and AFM (Bruker Dimension ICON-PT). The crystallinity of the films were analyzed using XRD (Philips X'pert diffractometer). Electrical analysis included sheet resistance vs. temperature (R vs. T), Hall measurements, and thermoelectric power. The R vs. T and the Hall measurements were taken using a simpler testing circuit utilizing the same thermal bridge/grease construction previously described, shown in Figure 4.2. All electrical characterizations were performed in the temperature regime of 300-10 K. Labview programs powered all of the electrical testing and data collection.

From the Hall data, the sheet carrier concentration n_H (cm^{-2}) and the mobility μ_H ($cm^2\ V^{-1}\ s^{-1}$) were extracted, using Equations 4.1 and 4.2.

$$n_H = \frac{IB}{V_H q t} \tag{4.1}$$

$$\mu_H = \frac{1}{n_H q R} \tag{4.2}$$

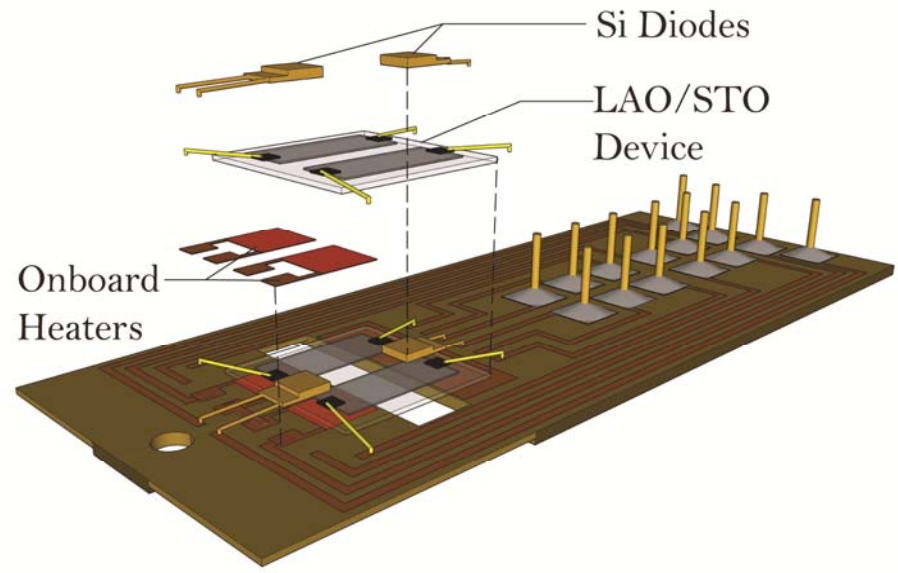

Figure 4.1 A pull-apart schematic of the thermoelectric testing setup, which illustrates the thermal isolation of the two sides of the device.

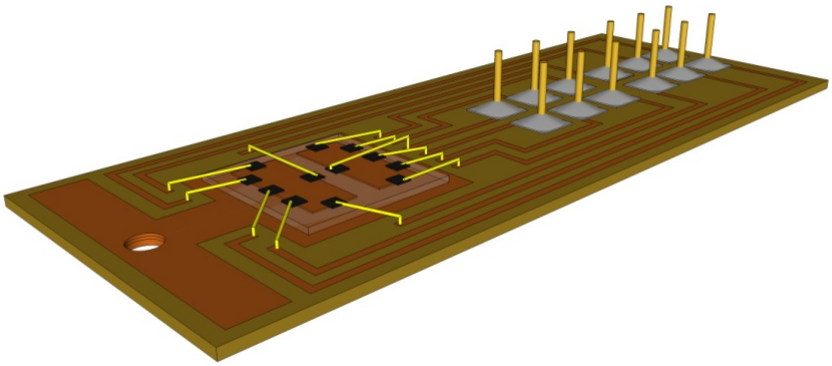

Figure 4.2 A schematic of the testing device used for the R vs. T and the Hall measurements, a more detailed description and image can be found in Section 3.3

In Equations 4.1 and 4.2, I represents the current that is passed longitudinally through the sample, B is the magnetic flux applied normal to the sample surface. The Hall voltage (V_H) is the voltage produced in the plane of the sample, but perpendicular to the current, the sign of the V_H indicates the dominant carrier type (see Figures 2.12, and 2.13 for greater detail). The symbols q, t, and R represent the charge of an electron, the thickness of the conducting channel, and the resistance, respectively. In two-dimensional systems the need exists to ignore the thickness (t) which then yields #/cm^2 for the units of carrier concentration (n_H), thus the Hall mobility (μ_H) is in units of cm^2/Vs. From the carrier concentration the activation energy (E_A) of the thermally activated carriers was calculated using Equation 4.3.

$$n_H = N_D \exp\left[\frac{-E_A}{2KT}\right] \tag{4.3}$$

In Equation 4.3, the symbols N_D, K, and T, represent the pre-exponential constant (proportional to the extrinsic carrier concentration), Boltzmann's constant, and the temperature. Using an Arrhenius plot of ln (n) vs. 1/T, the steep portion of the slope is equal to $-E_A$ /2K. From this graph the extrinsic and intrinsic carrier concentrations can easily be found, along with E_A (refer to Figures 2.14 and 2.15 for more details).

Thermoelectric testing was performed by allowing the system to reach thermal equilibrium, then applying power to isolated on-board heaters. The heater was cycled on and off at every temperature interval desired. At each set cryostat temperature the system was allowed to reach equilibrium. The process was then repeated. A Labview program

recorded the voltages developed and the diode temperatures. The data are then plotted as voltage difference (ΔV) against the temperature difference (ΔT). The Seebeck coefficient is easily extracted directly as the slope of the line, as the Seebeck coefficient S (μV/K) follows Equation 4.4

$$S = -\frac{\Delta V}{\Delta T} \tag{4.4}$$

The sign of the Seebeck coefficient reveals the dominant carrier, with negative and positive, relating to electrons and holes, respectively.

4.4 Results and Discussion

4.4.1 Structural Characterization

Film thicknesses were confirmed via optical profilometry, and indicated that the actual thickness was within 2-5% of the targeted values. Atomic force microscopy found the RMS roughness of the STO substrate and LAO film to be 3 and 4.6 Å, respectively (Figure 4.3), indicating a smooth and even film distribution.

XRD analysis revealed only STO peaks of the [100] family, as to be expected for the crystallographic direction of the substrate. No LAO peaks were observed, indicating an “epitaxial" thin-film (Figure 4.4). Although phi theta scans were not performed to prove heteroepitaxy, this can be easily assumed. The lattice parameters of the film and substrate are very similar, within 3%. Furthermore the films deposited were ultrathin. Thus the interfacial bonding energy can become sufficient to prevent dislocations.[7]

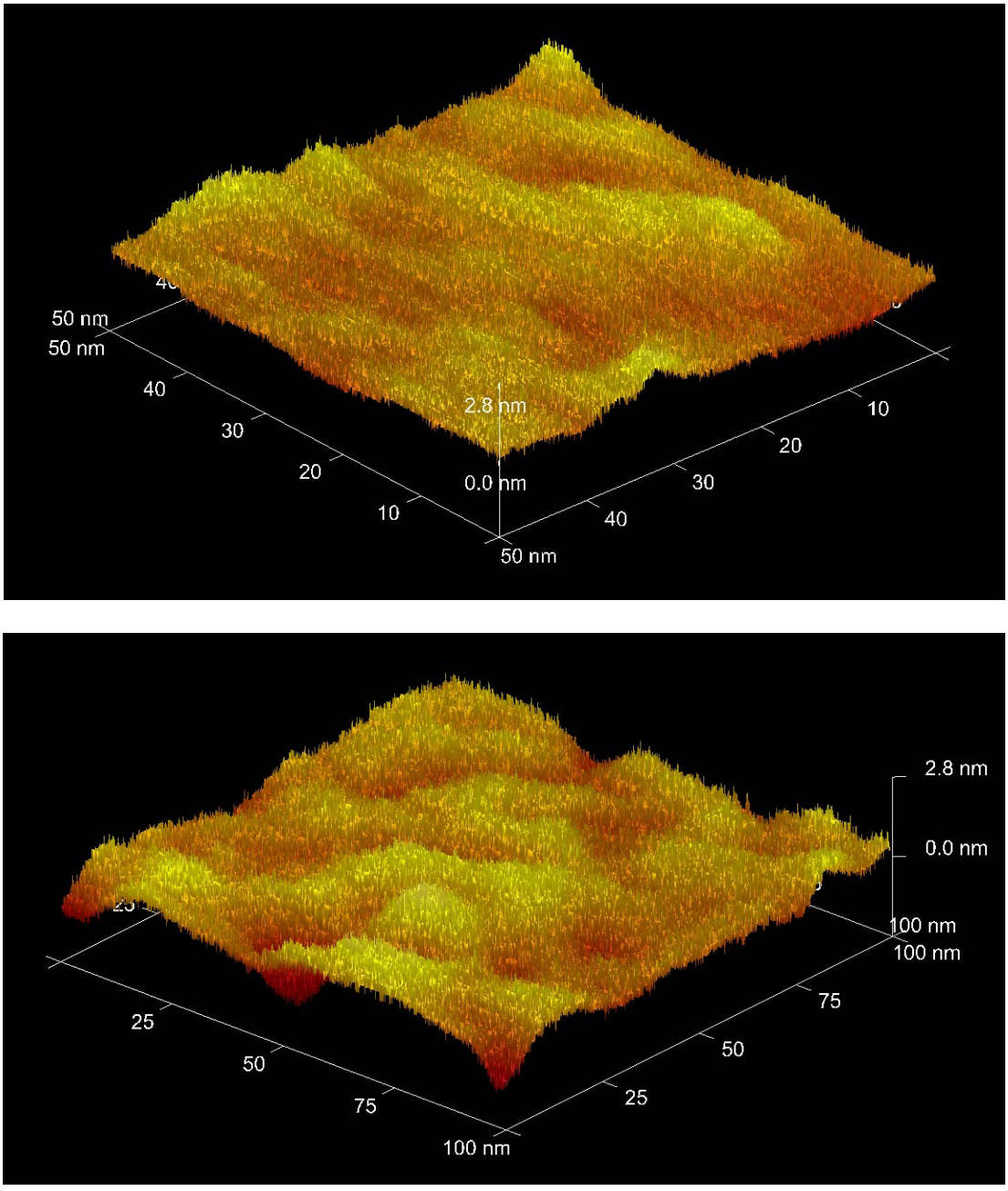

Figure 4.3 Atomic force microscopy (AFM) images of the STO substrate (Top), and the LAO film on STO (Bottom). The RMS roughness values found were 3 Å and 4.6 Å, respectively.

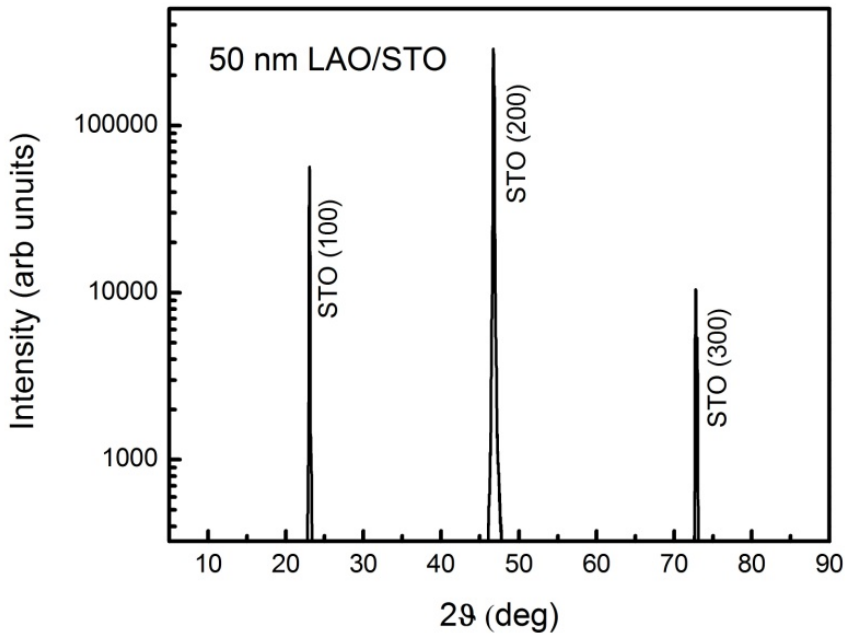

Figure 4.4 X-ray diffraction (XRD) scan of the 50 nm LAO film deposited on STO. The scan only reveals strong STO peaks of the [100] family, indicating epitaxial growth as no LAO peaks are present.

4.4.2 Electrical Characterization

4.4.2.1 Resistance and Hall measurements. Resistance vs. temperature (R vs.T) measurements were taken for all film thicknesses and for the control. The control STO had Pt contacts deposited under identical conditions (temperature, time, and oxygen pressure) as the LAO films. The control sample of the STO had an immeasurable resistance (<< 200 GΩ), along with the 100 nm LAO/STO film. However, the much thinner films of 50 and 5nm exhibited metallic conduction with low resistance. The sheet resistances vs. temperature results are presented in Figure 4.5. The 50 nm film possesses a resistance value that is three to four orders of magnitude less than that of the 5 nm film. Hall measurements were taken on both samples in the temperature range and magnetic field strength of, 300 K to 10 K, and ± 5 kG, respectively. The carrier concentrations (n), mobilities (μ), and the activation energies (E_A) were extracted from the Hall data, using Equations 4.1-3. The 50 nm film was found to possess large values for the carrier concentration and mobility, ~4.5 x 10^{16} cm^{-2} at 300 K, and ~5200 cm^2/Vs at 10 K, respectively. While the 5 nm film had a carrier concentration of 2.2 x 10^{14} cm^{-2} at 300 K, and a mobility of 500 cm^2/Vs at 10 K. (The signs of the Hall voltage and the Seebeck coefficient indicated the expected carrier to be electrons). A plot of the carrier concentrations and the mobilities is given in Figure 4.6.

4.4.2.2 Thermoelectric analysis. Following the procedures outlined in section 4.3.3, the Seebeck coefficients were extracted at 10-20 K increments, from 300 down to 10 K. The thermoelectric measurements revealed surprisingly high Seebeck coefficients (Figure 4.7). It is well known that the mobility of the charge carrier has a great impact on the resulting Seebeck coefficient.

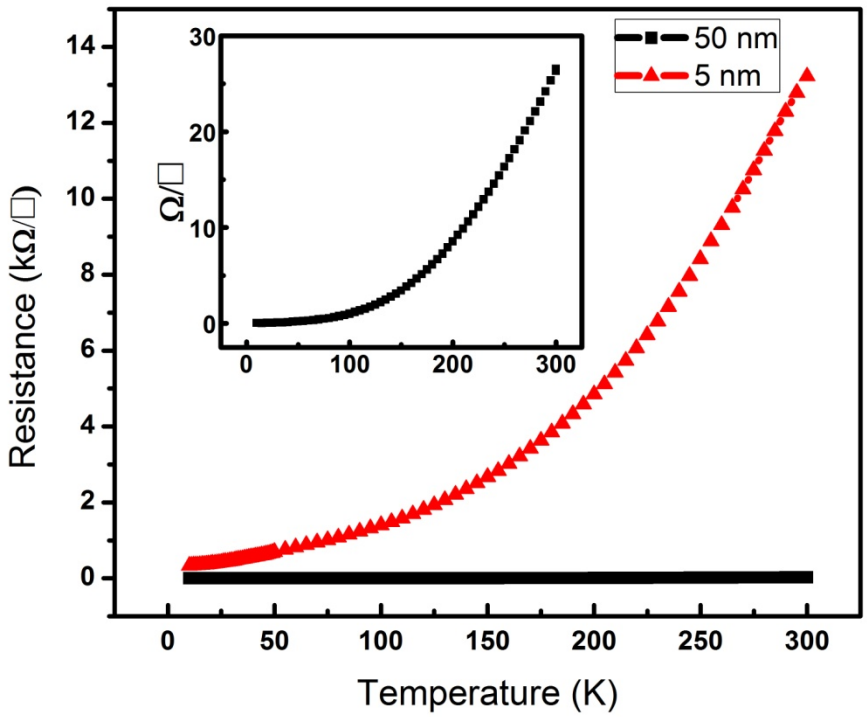

Figure 4.5 Plot of the sheet resistances vs. temperature. The inset illustrates the greatly reduced resistance of the 50 nm film. Note the Y-axis units of kilo-ohms for the 5 nm and ohms for the 50 nm films.

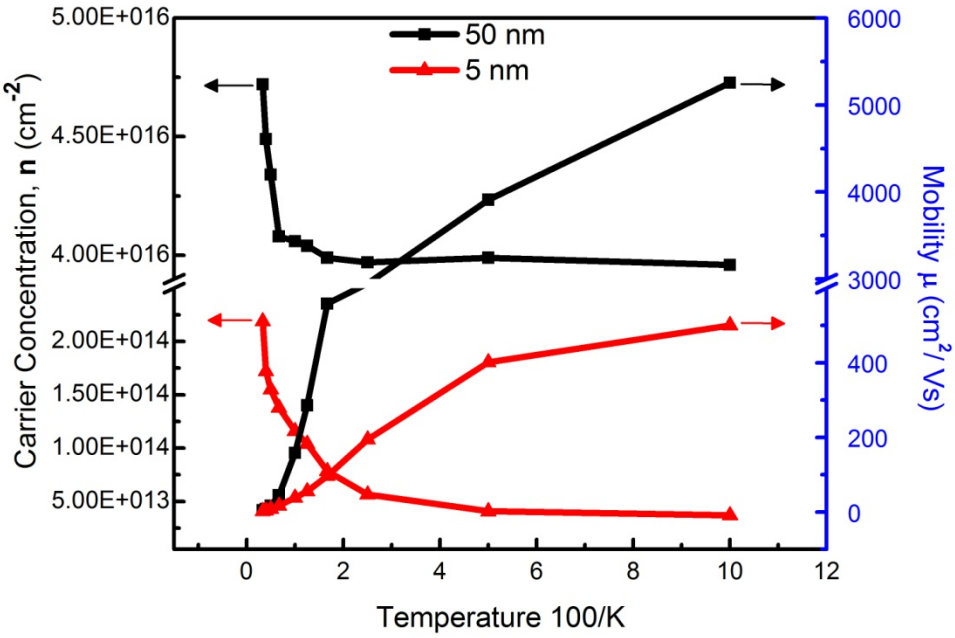

Figure 4.6 Double Y-axis plot showing the carrier concentrations (Left axis), and the mobility's (Right axis) of the 50 nm (125 UC) and the 5 nm (25 UC), the arrows point to their respective axis.

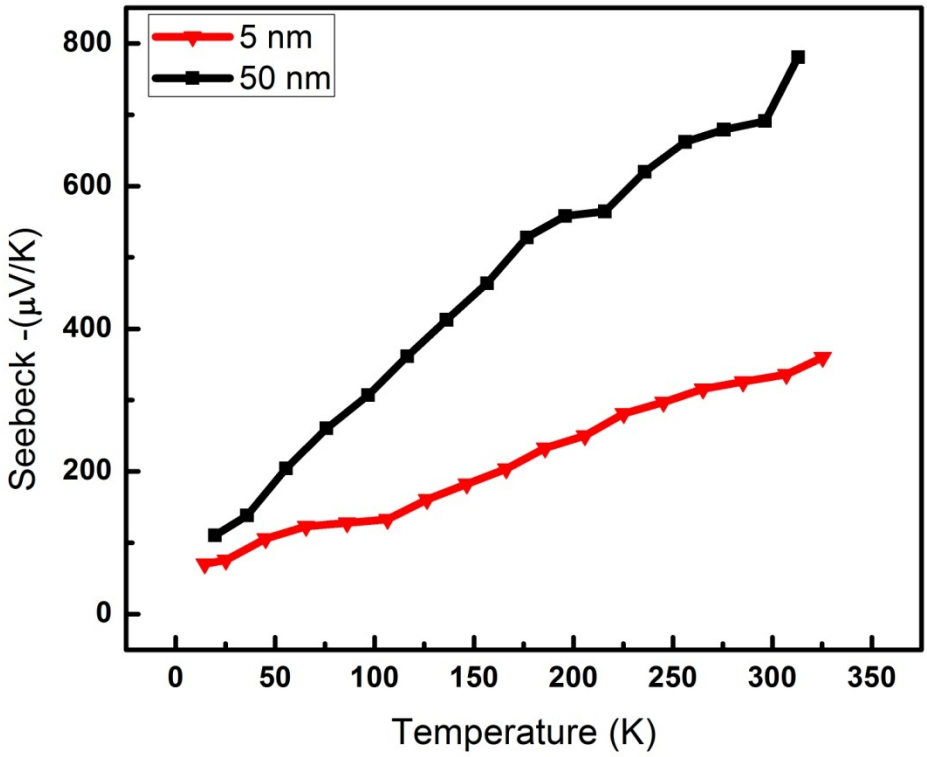

Figure 4.7 Absolute value of the Seebeck coefficient plotted against temperature. The figure illustrates the large Seebeck coefficients for the 50 and 5 nm films, which are 780 and 335 μV/K, respectively.

This is observed as the 50 nm film possessed much higher mobility and hence a much higher Seebeck coefficient, despite the higher number of carriers. The largest S values (Seebeck coefficients) found at room temperature for the 50 and 5 nm (125 and 25 unit cells) were ~780 and 335 μV/K respectively. These are extremely high values; the workhorse material for thermoelectric use is Bi_2Te_3 and its alloys, which possesses the 'high' Seebeck coefficient of 287 μV/K at 327 K. In a low dimensional superlattice, Ohta et al. have recently reported a "Giant" room temperature Seebeck coefficient of 850 μV/K with an STO/Nb:STO system.[2] Hence the results presented herein may also be referred to as giant Seebeck coefficients. Any Seebeck coefficient with a value that is above 100 μV/K is considered large. However the real values that are used to compare thermoelectric materials are the figure of merit Z (K^{-1}), and the unit less figure ZT, the Seebeck alone. These values both have the need to know the thickness of the conducting channel in order to calculate, as shown in Equation 4.5.

$$Z = \frac{S^2}{\rho k} \tag{4.5}$$

Here S, ρ, and κ are the Seebeck coefficient, resistivity, and thermal conductivity respectively. From the figure of merit Z, ZT is simply calculated by multiplying Z by the absolute temperature. However resistivity is in units of Ω-m. This is where the problem with 2DEG calculations of Z comes into play. Resistivity, ρ, is calculated by the relationship of resistance (R) and the dimensions involved, as shown in Equation 4.6.

$$\rho = \frac{Rwt}{l} \tag{4.6}$$

The dimensions of a three-dimensional conduction channel must be known; width *w*, length *l*, and the thickness *t*. It has been reported that the conduction channel thickness of such structures is one unit cell (.4 nm)[2], while in separate reports the conduction extends into 3-4 unit cells.[4] Still others have reported it to be less than the de Broglie wavelength.[8] For this study many different values of thickness were tried in an attempt to calculate the figure of merit values. The thickness values tried ranged from multiple unit cells down to the radius of a cation. None of the values used resulted in believable numbers for Z. For this thickness issue, and other complications with the substrate, the value of the Seebeck coefficient is solely used for the comparison of low-dimensional (2DEG) thermoelectric materials in the literature.[9]

4.5 Conclusions

In this paper we are the first to report on the encouraging results of the material system of lanthanum aluminum oxide thin films deposited on (100) strontium titanate, for thermoelectric power. The great results obtained from both the 5 nm (25 UC) thin film, and specifically the 50 nm (125 UC), indeed demonstrate the potential for this material system as a viable thermoelectric material. The results of the resistance, mobility, carrier concentrations, activation energies, and the Seebeck coefficients are summarized in Table 4.1.

The high Seebeck coefficients found in this report rival those of the current record holder for 2DEG thermoelectric power, Ohta et al.[2] As this group utilized a superlattice

Table 4.1 Summary of the experimental data collected throughout this study.

Symbol	Property	Temp	5 nm	50 nm	Units
R	Sheet Resistance	~10 K	337	0.03	Ω/□
R	Sheet Resistance	~300 K	13230	26.4	Ω/□
μ_H	Hall Mobility	~10 K	500.6	5254.4	cm^2/Vs
μ_H	Hall Mobility	~300 K	2.2	5.1	cm^2/Vs
n_H	Extrinsic Carriers	~10 K	2.2E+14	4.7E+16	$Carriers/cm^2$
n_H	Intrinsic Carriers	~300 K	3.5E+13	4.0E+16	$Carriers/cm^2$
E_A	Activation Energy	~200 K +	14.4	20.3	meV
|S|	Seebeck Coefficient	~20 K	73.1	110.4	μV/K
|S|	Seebeck Coefficient	~300 K	335.8	780.6	μV/K

structure to achieve their high values of S (850 μV/K), it stands to reason that the use of superlattices of the LAO/STO system could surpass this value. Also a more thorough investigation into the thicknesses of the LAO layer used should be performed. A certain thickness value will reach a maximum for the Seebeck, which needs to be found. Thus superlattices utilizing this thickness have great potential for actual device construction.

In conclusion a giant value of 780μV/K was recorded for a 125 unit cell LAO/STO 2DEG. This value along with all the values of S found concretely indicates the use of the LAO/STO 2DEG system as a viable thermoelectric material system. We are the first group to report on such positive results for the material system used. These findings and the suggestions contained herein will hopefully encourage other groups to further pursue the thermoelectric possibilities of this material system.

4.6 References

1. Dresselhaus, M. S.; Chen, G.; Tang, M. Y.; Yang, R. G.; Lee, H.; Wang, D. Z.; Ren, Z. F.; Fleurial, J. P.; Gogna, P., New directions for low-dimensional thermoelectric materials. *Advanced Materials* **2007,** *19* (8), 1043-1053.

2. Ohta, H.; Kim, S.; Mune, Y.; Mizoguchi, T.; Nomura, K.; Ohta, S.; Nomura, T.; Nakanishi, Y.; Ikuhara, Y.; Hirano, M.; Hosono, H.; Koumoto, K., Giant thermoelectric Seebeck coefficient of a two-dimensional electron gas in SrTiO3. *Nat Mater* **2007,** *6* (2), 129-134.

3. Ohtomo, A.; Hwang, H. Y., A high-mobility electron gas at the LaAlO3/SrTiO3 heterointerface. *Nature* **2004,** *427* (6973), 423-426.

4. Chambers, S. A., Understanding the mechanism of conductivity at the LaAlO 3/SrTiO3(001) interface. *Surface Science* **2011,** *605* (13-14), 1133-1140
.

5. Dresselhaus, M. S.; Chen, G.; Tang, M. Y.; Yang, R.; Lee, H.; Wang, D.; Ren, Z.; Fleurial, J. P.; Gogna, P., New directions for low-dimensional thermoelectric materials. *Advanced Materials* **2007,** *19* (8), 1043-1053.

6. Ohta, H., Thermoelectrics based on strontium titanate. *Materials Today* **2007,** *10* (10), 44-49.

7. Singh, R. K.; Narayan, J., Pulsed-laser evaporation technique for deposition of thin films: Physics and theoretical model. *Physical Review B* **1990,** *41* (13), 8843-8859.

8. Ohta, H., Two-dimensional thermoelectric Seebeck coefficient of SrTiO3-based superlattices. *Physica Status Solidi (b)* **2008,** *245* (11), 2363-2368.

9. Pallecchi, I.; Codda, M.; Galleani d'Agliano, E.; Marré, D.; Caviglia, A. D.; Reyren, N.; Gariglio, S.; Triscone, J. M., Seebeck effect in the conducting LaAlO_{3}/SrTiO_{3} interface. *Physical Review B* **2010,** *81* (8), 085414.

CHAPTER 5

THE FORMATION AND STUDY OF SWITCHABLE 2DEGs USING THE KN/STO SYSTEM

5.1 Abstract

Since the advent of a high mobility, all-oxide two-dimensional electron gas (2DEG) at the interface of two band insulators (LAO/STO)[1], there has been a worldwide pursuit to understand the metallic conduction mechanism/s. The mechanism is still not fully understood and is hotly debated. Regardless the elusive mechanism/s involved the system has great potential for nanoelectronics, all-oxide field effect transistors, high temperature superconductivity, and as the author revealed in Chapter 4, thermoelectric power.

Before the majority of these possibilities can be realized for practical device application the 2DEG require the ability of switching the state of conduction at room temperature. LAO/STO 2DEG have been shown to be switchable in the milli-Kelvin range.[2] It has also been shown that an AFM tip can write and erase conducting channels with films below the critical thickness (4UC).[3] Unfortunately neither one of these methods is device practical.

However Wang et al. have proposed theoretical work indicating that the use of a ferroelectric thin film on STO could possess switchable behavior, via an external electric field.[1, 2] Superconductivity and possibly multiferroic properties were also proposed at low temperatures. In the theoretical work, the material potassium niobate (KN) was suggested as the optimal film choice. Hence, the material system of ultrathin films of KN on STO was chosen to study in great depth. The results obtained herein are the first to show experimentally that the resistance of the KN/STO system possesses a great dependence on electric field. The samples prepared also show an unusual metal insulator transition (MIT) that supports the low temperature superconductivity prediction. We have shown experimentally that the theory of ferroelectric 2DEG device practicality is plausible. This report is the first to indicate these findings.

5.2 Background and Introduction

5.2.1 Lanthanum Aluminum Oxide/ Strontium Titanate 2DEGs

Since Ohtomo et al. first created a 2-dimensional electron gas (2DEG) at the interface of the two band insulators using thin films of lanthanum aluminum oxide (LAO) on Ti terminated strontium titanate (STO), there has been a worldwide pursuit to both create and understand the mechanisms involved. The actual cause of the metallically conducting layer is still hotly debated. It is well known that LAO possesses polarity in its layers (100); the leading theory suggests that this polarity would cause a surface divergence. This divergence is referred to as a polar catastrophe, which is energetically unfavorable. Thus either an electronic or an atomic restructuring must occur at the interface. The other two main theories are oxygen vacancies which are known to make

STO conductive and the interdiffusion of cations namely lanthanum into the STO which is a known donor. [3] Regardless the mechanism/s involved there is great potential for these nanostructured 2DEGs. Such as nanoelectronics, all-oxide field effect transistors, high temperature superconductivity, and many others. Furthermore as the author has shown in the previous chapter these 2DEGs could also be used for thermoelectric power. One of the major obstacles to overcome before most of these applications can be realized is the ability to switch the conductance of the channel off and on. Although the LAO/STO 2DEGs have been shown to be switchable in the milliohm range with an external electric field.[4] It has also been shown that when the LAO film is below the critical thickness (less than 4 unit cells) that a conduction channel can be written and erased with a charged AFM tip.[5] [6] Neither of these two switching mechanisms have any potential for real world device capability.

5.2.2 Theoretical Prediction of Switchable Ferroelectric 2DEGs

Wang et al. have theoretically calculated that the use of a ferroelectric film (namely potassium niobate, KN) on STO may produce a switchable 2DEG. [1, 2] In the proposed case the application of an external electric field would cause the noncentrosymmetry of the multivalant cation (Nb) to move either toward or away from the interface, thus moving the free electrons. This would in turn reduce or increase the resistance of the channel, thus creating a switchable channel. An illustration of the theory can be seen in Figure 5.1. It was emphasized in that unlike the LAO/STO 2DEGs which needed a Ti terminated surface the KN/STO would need an Sr termination to allow the Nb to reside at the interface. The importance of an atomically abrupt and sharp interface

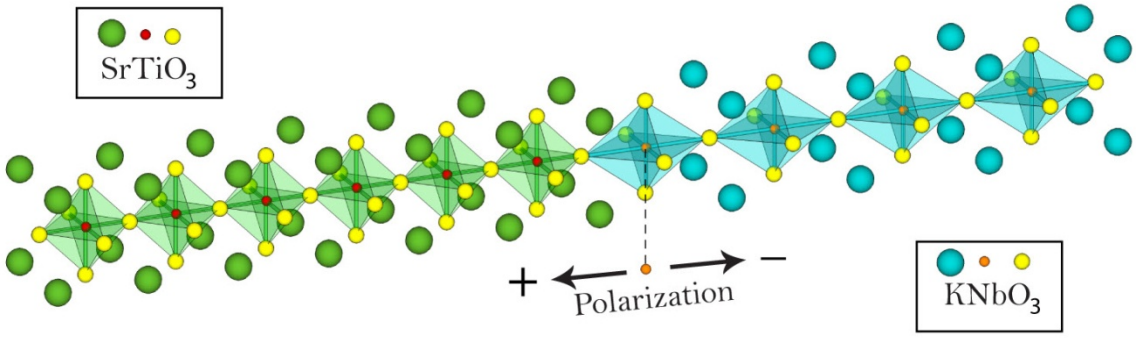

Figure 5.1 Schematic illustration of the proposed device. This schematic enables the visualization of the STO cubic phase, and the orthorhombic phase of the KN. The noncentrosymmetry of the KN phase gives the Nb cation a degree of freedom to move when an electric field is applied.

is also stressed in the article by Wang et al. Moreover low temperature superconductivity and possible multiferroic properties were also predicted.[2]

The material system of KN films grown on STO substrates was thoroughly researched in this study. To the knowledge of the authors, the successful creation of such switchable devices has not yet been accomplished at practical temperatures with any 2DEG system. In this paper we report the successful creation of such devices with the KN/STO material system. The samples reveal a dramatic shift in resistance when an external bias is applied, thus proof of concept for the theoretical work proposed by Wang et al. is validated.

5.3 Experimental Procedure

5.3.1 Thin Film Production

Following the work done by Ohtomo et al. for the construction of his LAO/STO 2DEGs, a six-probe Hall geometry was chosen for the construction and testing of the KN/STO 2DEGs.[7] This was accomplished using a two-step contact shadow mask procedure utilizing a theta z mask aligner. A schematic of the mask aligner is shown in Figure 3.2. In order to ensure interfacial contact, an overlapping contact design was chosen where the Pt was deposited halfway on and off the thin film. Experience has also shown that the use of higher laser fluence will cause the Pt to make contact with the substrate surface, thus the interface.

In order to give the (100) STO the required strontium terminated surface, preferential Sr etching was first performed (HF), yielding a Ti surface. Next utilizing a solid Sr metal target, a monolayer of Sr was deposited via PLD. The KN films were

deposited using a near perfect density target (see section 2.3 for target preparation details). Following the KN, the Pt contacts were deposited. All three depositions were performed without the breaking of the PLD vacuum chamber. The laser fluences used were 4.7, 3.5, and 5.5 J cm^{-2} for the Sr, KN and Pt targets, respectively. All of the films were deposited at 750° C, with an oxygen partial pressure of 10^{-6} torr. KN films of 100, 50, 25, and 5 nm were produced (several of each thickness). Control films were produced under the same conditions, including the use of a Ti terminated substrate and an STO substrate with only Pt contacts deposited.

5.3.2 Testing Circuit Design

PCB circuit testing circuits were designed to hold the devices securely and enable the ability for wire bonding (Figure 5.2). The testing circuits were designed to fit the stage of a liquid helium closed cycle cryostat. A direct copper thermal contact was created between the top and bottom of the testing board; see section 2.5.3 for the detailed procedures on the testing circuit construction.

The same testing circuit boards utilized for the LAO/STO 2DEGs were used for this study of the KN/STO system, with some minor changes. The alterations made were the addition of a contact pin to the copper plate underneath the substrate for a bias connection. The other addition was that of simply placing a thick copper plate with a contact pin directly on top of the cover glass. The placements of the bias plates enabled the ability to apply a reversible electric field to the thin films without electrical contact. A simplified schematic of the R vs. E setup is shown in Figure 5.3.

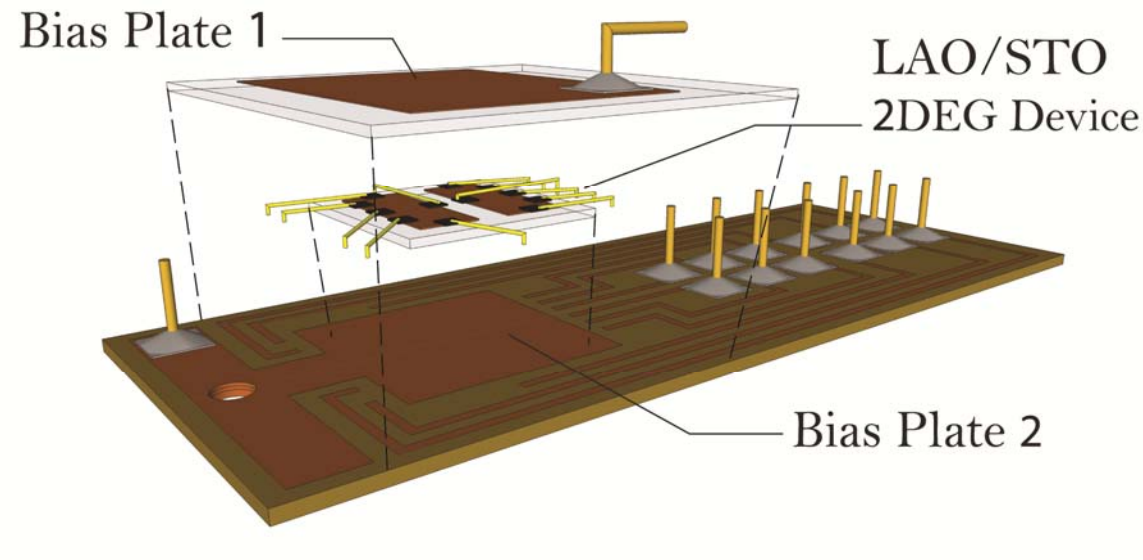

Figure 5.2 Schematic of the KN/STO mounted to the testing circuit. The figure illustrates the positions and the separations of the DC bias plates.

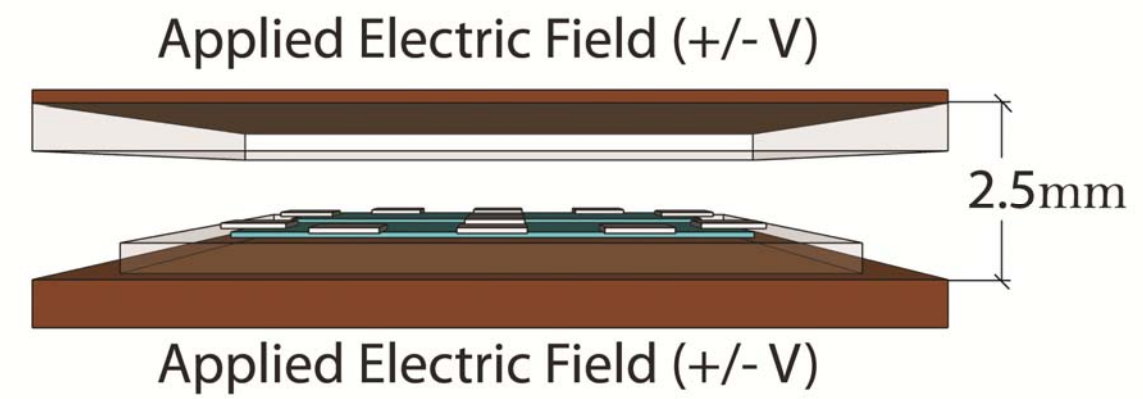

Figure 5.3. Illustration (not to scale) of how the external electric field was applied. Note the separation between the bias plates was 2.5 mm. The distance between the top of the device and the bottom of the cover glass is 1.5 mm (not indicated).

5.3.3 Characterizations Utilized

The thickness and surface morphology of the KN films were examined using a profilometer (Tencor P-10), and an AFM (Bruker Dimension ICON-PT). The crystallinity of the films was analyzed using XRD (Philips X'pert diffractometer).

Electrical analysis included sheet resistance vs. temperature (R vs. T), Hall measurements, and resistance vs. applied external electric field (R vs. E). All of the electrical characterizations were performed in the temperature range of 300-10K.

The resistances vs. external electric field measurements were performed by applying a field with a DC source, returning the field to zero, and then switching the bias. The separation between the charged copper plate under the substrate, and the copper plate on top of the cover glass was 2.5 mm. Using the known separation and the voltages applied the field strength was easily found. The thicknesses of both the substrate and the cover glass were a half a millimeter, thus leaving a 1.5 mm gap between the film and the glass. The measurements were taken under vacuum in a closed cycle liquid helium cryostat.

5.4 Results and Discussion

5.4.1 Structural Characterization

Film thicknesses were confirmed via optical profilometry, and indicated that the actual thickness was within 2-5% of the targeted values. Atomic force microscopy found the RMS roughness of the STO substrate and KN films to be 3 and 3.3 Å, respectively. The AFM films are shown in Figure 5.4; the large particles seen on the KN film surface were identified as dust, as they were easily moved with the AFM tip.

XRD analysis revealed only STO peaks of the [100] family, as to be expected for the crystallographic direction of the substrate, with no KN peaks were observed (Figure 5.5). Phi-theta scans were not able to be performed in order to prove heteroepitaxy. The films however can be deduced as heteroepitaxial. The lattice parameters are nearly a perfect match (STO .3905 nm, KN .3973 nm), and the ultrathin nature of the film. It should also be noted that an abrupt, sharp terraced interface *was not* observed via AFM. This is important as an abrupt interface is indicated to be essential in the theoretical work for this material system.[1, 2] This sharp and abrupt interface is also considered by many as essential for the success of the prototypical all-oxide 2DEG (LAO/STO).[1,2,7,8,9,10] The lack of the sharp interface is further evidence of a conduction pathway that is not quantum confined (the same results were also shown in Chapter 3).

5.4.2 Electrical Characterization

Resistance versus temperature measurements were taken for all film thicknesses and for the control. The resistances of control STO, Ti terminated surface, the 100 nm, and the 50 nm films were all immeasurable (<< 200 GΩ). However some very intriguing resistance vs. temperature (2 & 4-probe) results for all of the 25 and 5 nm samples were obtained. The films behaved as an insulator from room temperature down to about 25-35 K, at which point a maximum was reached. Following this maximum, the resistance reduces drastically, as shown in Figure 5.6. This apparent transition (similar to a metal-insulator transition) was first considered to be an instrumental error. This was soon ruled

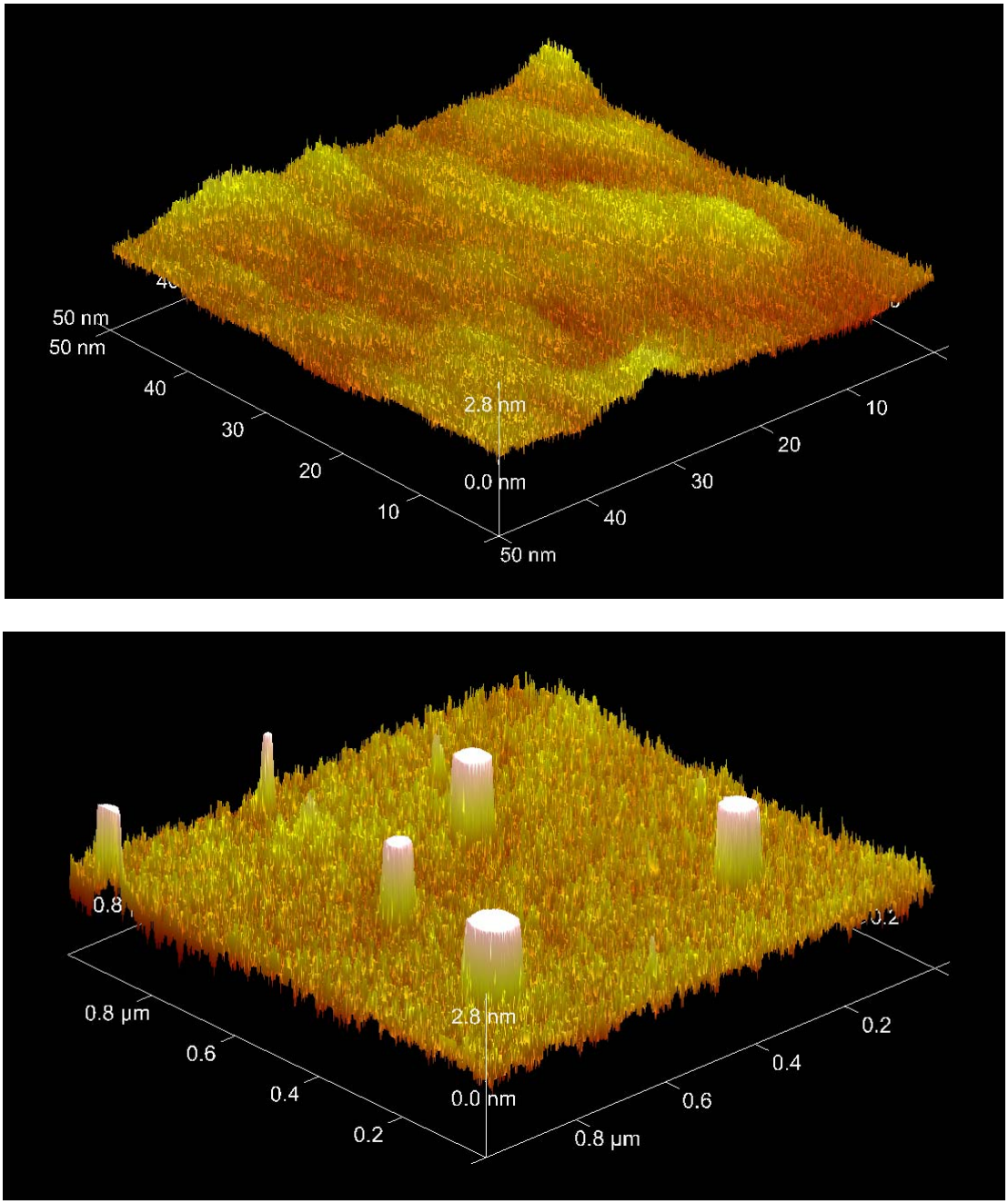

Figure 5.4 Atomic force microscopy (AFM) images of the STO substrate (Top), and a 25 nm KN film on STO (Bottom). The RMS roughness values found were 3 Å and 3.3 Å respectively. The peaks on the KN film were identified as dust, due to their movement from the AFM tip.

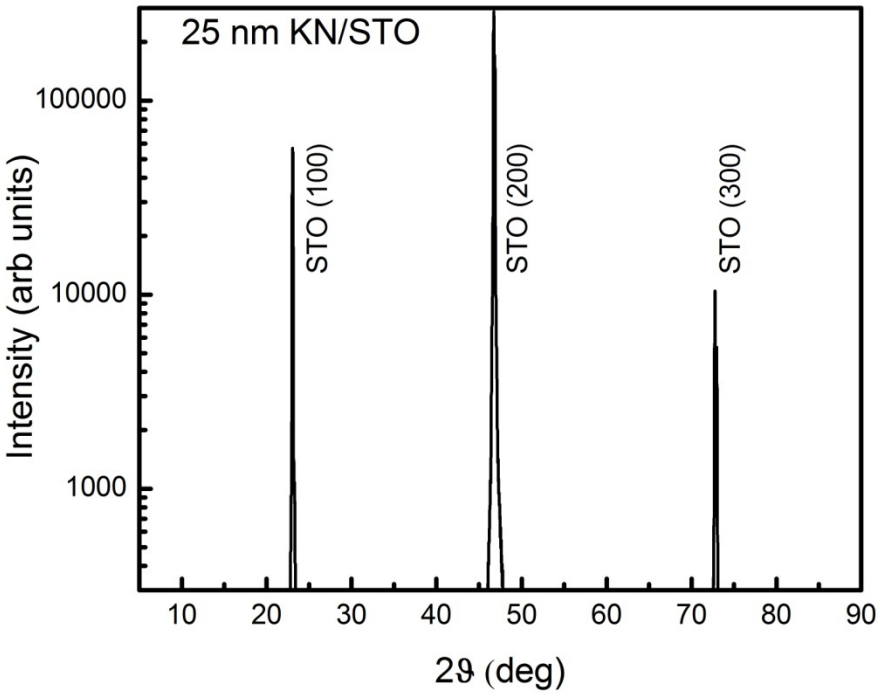

Figure 5.5 X-ray diffraction (XRD) scan of the 25 nm KN film deposited on STO. The scan only reveals strong STO peaks of the [100] family, with no KN peaks, indicating the likelihood of epitaxial growth.

out after many different instrumental configurations were used. These configurations included both 2 and 4 probe measurements along with the use of a highly sensitive Keithley Electrometer (6514) which is accurate up to 200 GΩ. From Figure 5.6 it can easily be seen that this resistance value was never approached. Hence it is only reasonable that the transition observed indeed exists. Thus the transition is a property of the material system, namely the interface, as neither STO nor KN behaves in this way alone.[11] Unfortunately the ability to go below 10 K was not available. but the steepness of the slopes, indicate the prediction of low temperature superconductivity to be correct.[2]

The room temperature resistances for the film thicknesses of the 25 nm A/B, and the 5 nm A/B were found to be, 265/194 kΩ, and 142/166 kΩ, respectively. These relatively high resistance values prevented successful Hall measurements; hence carrier concentrations and the mobilities were not able to be calculated.

The resistance of the samples demonstrated a great dependency on the electric field that was applied. These results resemble that of a field effect transistor (FET). Furthermore a hysteresis type behavior was observed when the electric field direction was reversed, indicating the polarization of the film. This is to be expected in a piezoelectric material such as potassium niobate. An example of R vs. E revealing this hysteretic behavior can be seen in Figure 5.7. In order to rule out the possibility of false readings due to the experimental setup, well functioning premade LAO/STO 2DEGs (Chapter 3) were tested in the same testing fixtures under the same conditions. There was no effect on the resistance of these films with the application of the electric field. This control experiment indicates that the field dependency of the KN/STO heterostructure is

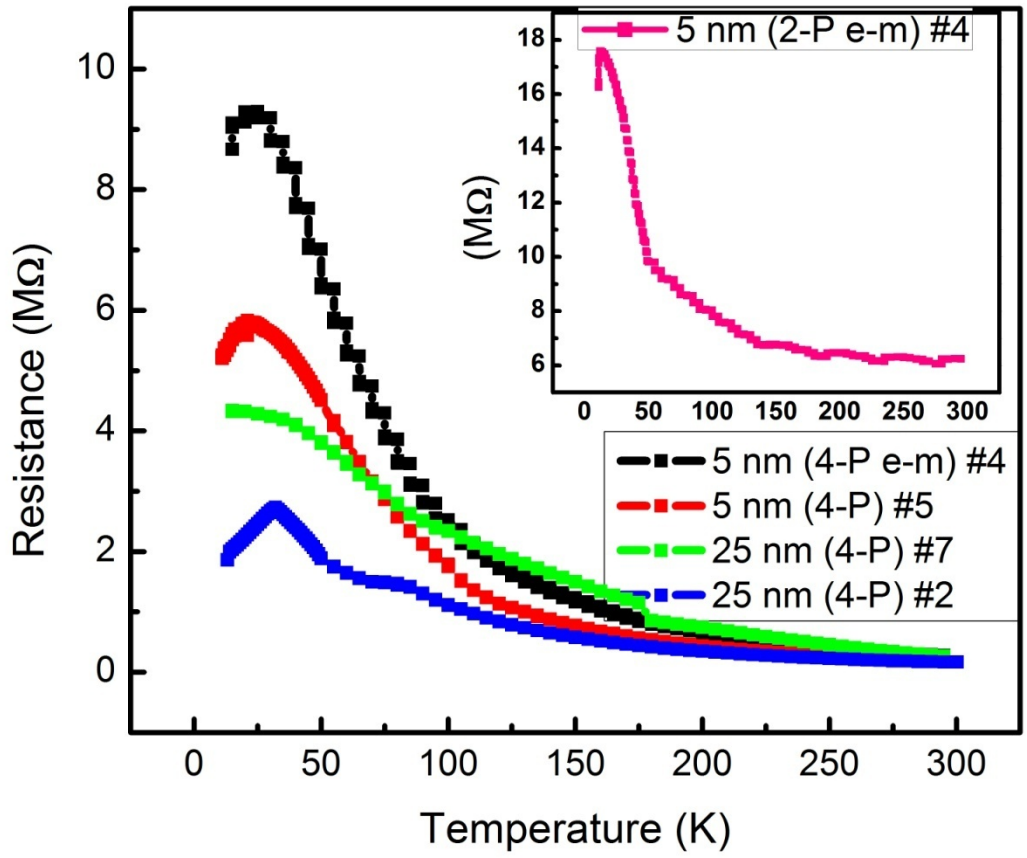

Figure 5.6 Plots of the resistance as a function of temperature for all of the KN/STO samples. The plot illustrates the pronounced metal-insulator-transitions between 35 and 25 K. The abbreviations of 4-P and 2-P stand for 4 and 2-probe configurations, the # at the end of the legend refers to the sample #, lastly e-m stands for the use of an electrometer.

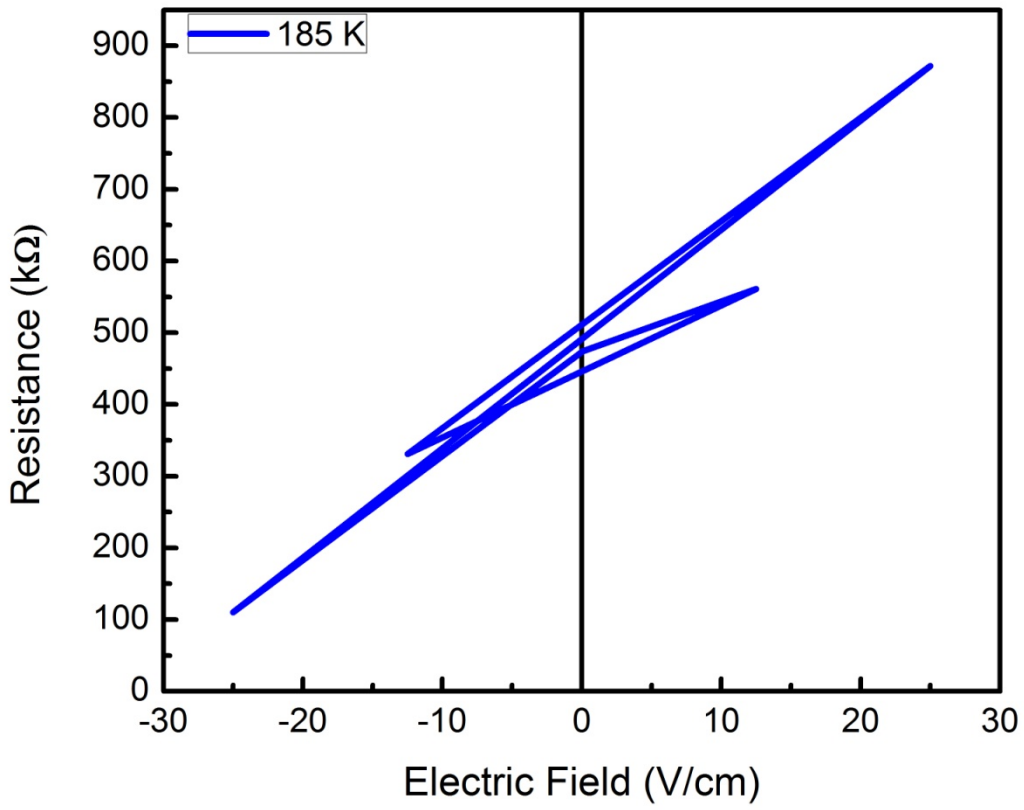

Figure 5.7 Plot of the resistance versus the applied electric voltage, illustrating the strong dependence on field strength, as well as the hysteretic nature of the film.

indeed a material property. Furthermore these results are the first to confirm the concepts proposed in the theoretical work of Wang and Narijan.[1, 2]

Despite these exciting results it must be noted that an unexplainable phenomenon was observed. Occasionally while switching the bias directions the resistance changes from a positive value to an unbelievable negative value (at many temperature values). An example of this phenomenon is shown in Figure 5.8.

Many theories were proposed to explain the obvious false readings. A short between the bias plates was suspected as the cause, but due to the separation and the presence of vacuum, this could only occur via an arcing mechanism. Such an arcing event would leave evidence on the substrate and/or the underside of the cover glass. No such evidence was found. Reason then led to the idea that a current was passing through the substrate and creating a current flow. However STO is known to possess a high dielectric constant of 400 at room temperature and an extremely high value of ~30,000 at low temperatures, thus ruling this possibility out. It was then noted that contact was being made with both the top and bottom of the KN film. This led to the thought that a current was flowing from one side of the polarized film to other. A new 5 nm sample was deposited with the Pt contacts directly on the substrate; hence contact was only made at the interface. However this film produced similar results for both the R vs. T and the R vs. E measurements, once again ruling out this possibility.

Unparallel bias plates causing the field to have an x-component was thought to have been driving a current. Despite the fact that there was no mechanism to complete the circuit, this hypothesis was explored. The top bias plate was tilted at several angles and in

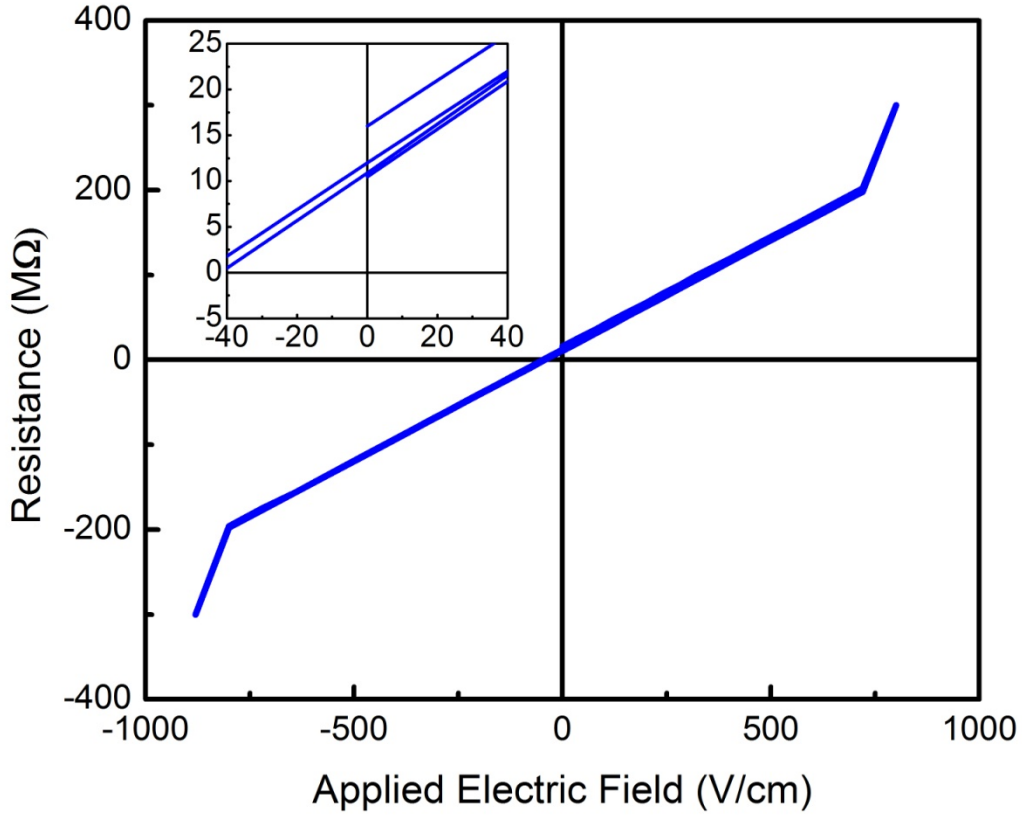

Figure 5.8 Plot showing the occasional phenomenon of negative resistance recorded. The inset is a zoomed in section of the larger plot, illustrating positive resistance at low fields and a hysteretic-type behavior.

several directions to intentionally create a non-uniform field. Regardless, the angle or the direction of tilt had no noticeable effect.

The only explanation left was that the presence of the bias was occasionally causing the instruments to give false readings. Thus different instrument configurations were tried including 2 and 4 probe resistance setups. The use of extremely sensitive equipment such as the aforementioned electrometer was also utilized, with no change. The cause of the negative resistance occasionally observed still remains a mystery.

5.5 Conclusions

In conclusion, we are the first to have shown that a switchable all-oxide 2DEG can be constructed with the use of a ferroelectric film. Such all-oxide FETs have great possibility for real world device use. Although other groups have shown 2DEGs to have a switchable behavior, the temperature (mK) at which this occurs is impractical for the realization of devices.[4] The results in this study have shown room temperature field dependence, which is a major requirement for device realization. Furthermore these results have provided proof of concept for the theorized system proposed by Wang et al.

This material system needs further investigation, and it is proposed that the use of superlattice structures could greatly improve the performance, specifically by reducing the resistivity without a bias present. The strange negative results should also be studied by other groups in order to see if it is indeed just instrumental error.

In closing we have shown the great potential of this system and hope to inspire more research in ferroelectric 2DEG construction. The author would like to thank Y. Wang and M. Naranjan for their motivating theoretical work.

5.6 References

1. Niranjan, M. K.; Wang, Y.; Jaswal, S. S.; Tsymbal, E. Y., Prediction of a switchable two-dimensional electron gas at ferroelectric oxide interfaces. *Physical Review Letters* **2009,** *103* (1).

2. Wang, Y.; Niranjan, M. K.; Jaswal, S. S.; Tsymbal, E. Y., First-principles studies of a two-dimensional electron gas at the interface in ferroelectric oxide heterostructures. *Physical Review B - Condensed Matter and Materials Physics* **2009,** *80* (16).

3. Chambers, S. A., Understanding the mechanism of conductivity at the LaAlO 3/SrTiO3(001) interface. *Surface Science* **2011,** *605* (13-14), 1133-1140.

4. Caviglia, A. D.; Gariglio, S.; Reyren, N.; Jaccard, D.; Schneider, T.; Gabay, M.; Thiel, S.; Hammerl, G.; Mannhart, J.; Triscone, J. M., Electric field control of the LaAlO3/SrTiO3 interface ground state. *Nature* **2008,** *456* (7222), 624-627.

5. Park, J. W.; Bogorin, D. F.; Cen, C.; Felker, D. A.; Zhang, Y.; Nelson, C. T.; Bark, C. W.; Folkman, C. M.; Pan, X. Q.; Rzchowski, M. S.; Levy, J.; Eom, C. B., Creation of a two-dimensional electron gas at an oxide interface on silicon. *Nature Communications* **2010,** *1*, 94.

6. Cen, C.; Thiel, S.; Hammerl, G.; Schneider, C. W.; Andersen, K. E.; Hellberg, C. S.; Mannhart, J.; Levy, J., Nanoscale control of an interfacial metal-insulator transition at room temperature. *Nature Materials* **2008,** *7* (4), 298-302.

7. Ohtomo, A.; Hwang, H. Y., A high-mobility electron gas at the LaAlO3/SrTiO3 heterointerface. *Nature* **2004,** *427* (6973), 423-426.

8. Reyren, N.; Thiel, S.; Caviglia, A. D.; Kourkoutis, L. F.; Hammerl, G.; Richter, C.; Schneider, C. W.; Kopp, T.; Ruetschi, A. S.; Jaccard, D.; Gabay, M.; Muller, D. A.; Triscone, J. M.; Mannhart, J., Superconducting interfaces between insulating oxides. *Science* **2007,** *317* (5842), 1196-1199.

9. Gariglio, S.; Reyren, N.; Caviglia, A. D.; Triscone, J. M., Superconductivity at the LaAlO3/SrTiO3 interface. *Journal of Physics Condensed Matter* **2009,** *21* (16).

10. Guisinger, N. P.; Santos, T. S.; Guest, J. R.; Chien, T. Y.; Bhattacharya, A.; Freeland, J. W.; Bode, M., Nanometer-scale striped surface terminations on fractured SrTiO3 surfaces. *ACS Nano* **2009,** *3* (12), 4132-4136.

11. Xu, Y., *Ferroelectric materials and their applications*. North-Holland ; Elsevier Science Pub. Co.: Amsterdam ; New York,New York, 1991.

CHAPTER 6

CONCLUDING REMARKS

6.1 LAO/STO 2DEGs

Against popular belief, the optimal LAO film thickness was found to be around 50 nm, as the 100 nm film was immeasurable and the 50 nm (125 UC) film greatly outperformed all of the other thicknesses (25,10, and 5 nm). An atomically abrupt and sharp interface was not observed, without any terraced structure. Despite the 'imperfect' surface, the values of resistance, mobility, and carrier concentrations that were found are quite comparable to other reported values. This evidence demonstrates that the assumption and the preparation of an atomically abrupt interface are not required. Furthermore these results illustrate that the conduction channel is not a quantum confinement, but several mechanisms are at work.

6.2 Thermoelectric Power with LAO/STO 2DEGs

We are the first to report that the LAO/STO system has great potential for thermoelectric power generation. The TEP measurements for both the 50nm (125 UC), and the 5nm (25 UC) revealed high Seebeck coefficients, 780 and 336 μV/K, respectively.

The high Seebeck coefficients that were recorded rival the current record holder for 2DEG thermoelectric power, (Ohta). His group utilized a superlattice structure of STO/Nb:STO in order to achieve the S value of 850 μV/K. In comparison the single interface that was tested within this study gave an S value of 780 μV/K. Logic reasons that a superlattice of LAO/STO has great potential exceed the aforementioned values.

In conclusion a giant value of 780μV/K was recorded for a 125 unit cell LAO/STO 2DEG. This value along with all the values of S found, concretely indicate the use of the LAO/STO 2DEG system as a viable thermoelectric material system. We are the first group to report on such results for the system used.

6.3 Switchable 2DEGs with the KN/STO System

We are the first to have shown that a switchable all-oxide 2DEG can be constructed with the use of a ferroelectric film. Furthermore this has never before been reported for this system, or any other oxide system at room temperature. The film resistances demonstrated a strong dependence on the applied field, as predicted. Such all oxide FETs present great possibility for real world devices. Now that the proof of concept has been achieved, further research needs to be done. This should include the construction of KN/STO superstructure devices, which should yield more exciting results. We would like to give credit to and thank Wang and Niranjan for their insightful theoretical work on the use of ferroelectrics to create such switchable 2DEGs.

6.4 Summary

In this thesis, oxide based 2-dimensional electron gases were investigated for alternative uses such as thermoelectric power. The requirement of an abrupt/sharp interface for successful LAO/STO 2DEGs was examined in an attempt to reveal quantum confinement as the dominant conduction mechanism. Furthermore novel 2DEGs based on a ferroelectric film (potassium niobate) were investigated for the plausibility of an all-oxide field effect transistor. Unique properties of the material systems studied and discovered in this thesis indicate their potential for many next generation devices.